FLOOD FREQUENCY AND INUNDATION ESTIMATIONS UNDER CLIMATE VARIABILITY IN EASTERN AUSTRALIA

Matthijs Gensen

29 August 2014

UTAS

UNIVERSITY OF TWENTE.

Flood Frequency and inundation estimation under climate variability in Eastern Australia

Bachelor Thesis

Author:

Matthijs R.A. Gensen

Bachelor Civil Engineering University of Twente

Supervisors University of Tasmania:

Prof. Stewart Franks

Dr Christopher White

Supervisor University of Twente:

Juan Pablo Aguilar Lopez, MSc

Hobart, 29 August 2014

Photo frontpage: Queensland floods 2010/2011; ABC News, 22 September 2011

Summary

In this research a flood risk assessment was conducted for the Upper Mary River catchment. The Upper Mary River catchment is a relatively small non-coastal catchment area being 985 km^2 in size. The only usable stream gauge is the Bellbird Creek gauge as others were affected by a dam. In total 78 suitable yearly discharge peaks were derived and identified. It is expected that discharges in this catchment area are affected by various climate variability modes. This statement is tested for the El Niño Southern Oscillation (ENSO), Pacific Decadal Oscillation (PDO) and Interdecadal Pacific Oscillation (IPO).

At first an unconditional (independent of the phases of the climate variability modes) flood risk evaluation was conducted using all 78 yearly peaks. The resultant flood frequency curve can be compared to the conditional flood frequency curves which were calculated later. For the unconditional flood frequency multiple probability distributions were tested in order to find the best fitting distribution. It became evident that the Log Pearson type 3 distribution best fitted the data, therefore being used throughout the research. The resultant 100 year flood event and 1% annual exceedance probability is 3459 m^3/s.

To calculate the conditional flood frequency curves the phases of the different states of the IPO, PDO and ENSO were identified. For the IPO three phases were distinguished since 1920, two positive phases from 1920 to 1944 and from 1978 to 1998 and one negative phase from 1946 to 1976. The PDO and ENSO states were identified using climate indices and dividing them into positive, neutral and negative years.

Subsequently the discharge peaks were divided into the years corresponding to the identified climate states. Using these discharge series the conditional flood frequency curves were determined. It was expected that all three climate variability modes would show an effect, but for the IPO no signal was found. The PDO and the ENSO showed similar effects in which the negative PDO phase and the La Niña phase had a higher 100 year flood event, respectively 5008.9 and 5179.2 m^3/s opposed to 3010.6 and 3439.5 m^3/s for the positive states.

It is unequivocal that these variabilities lead to uncertainty in flood risk analyses. This uncertainty was evaluated by calculating random 100 year floods in a Monte Carlo simulation using different data lengths considering only the ENSO variability. When using a data series consisting of only 30 years the 95% bandwidth was found to be between $2.0 * 10^3$ and $8.8 * 10^3$ m^3/s. Applying a considerably longer data length of 200 years the remaining uncertainty remained large: a 5% chance of the true value of the 100 year flood event being under $2.7 * 10^3$ m^3/s or over $5.3*10^3$ m^3/s.

The calculated 100 year flood events were applied in a built HEC-RAS model in order to estimate flood inundations. It was found that little variety in flooded area would occur under the different climate variability states. This is caused by the specific bathymetry of the researched area. In terms of flood inundation heights larger differences were found, with the La Niña 100 year flood event having 2.0 metres additional inundation in comparison to El Niño's 100 year flood event.

Besides climate variability, future climate change is a potential source of error in flood risk analyses. It was found that for the area of interest, Eastern Australia and Southeast Queensland in specific, little quantitate predictions of climate change in terms of extreme events have been made. Researches with qualitative predictions also vary in their expected future changes. Some expect a decreased flood risk, whereas others expect an increased flood risk. The few quantitate predictions were applied to the Upper Mary River catchment. However a significant change in flood risk could not be determined.

Preface

This report is the product of the research for my bachelor thesis. Stationed at the University of Tasmania I researched flood risks for 10 weeks. Although the area of study, Southeast Queensland, is over a thousand kilometres away the resources of the University of Tasmania were helpful to complete the research.

During the first week of the research it already became clear the research would be fairly different to what was intended in the first research proposal. With a lesser focus on future climate the aim of the research became more feasible. The first few weeks were dominated by programming. The models were up and running earlier than expected and this gave me the opportunity to clearly select the most suitable data and gain the best possible results.

In the process of conducting the research and creating this report I have learned a lot. This contributed to my whole visit to Tasmania being a great experience. I would like to thank all people for any kind of help and support. Firstly I would like to thank Crispin Smythe from the Sunshine Coast Regional Council for providing all data for the Upper Mary River catchment. Secondly I thank Juan Pablo Aguilar Lopez from the University of Twente for his feedback on the preliminary reports. Furthermore I thank Christopher White of the University of Tasmania for all his help. At last I would like to thank Stewart Franks for his help and for hosting me at the University of Tasmania.

Contents

1 Introduction

Australia experiences a large variety of climates throughout; from the arid and semi-arid areas in the centre to the tropical climate in the north. This extreme variety of climates can be seen in Figure 1-1. A phenomenon with a huge impact on the climate in Australia is known as the El Niño-Southern Oscillation (ENSO). The highly seasonal rainfall pattern is influenced by the seasonal abnormality of the ENSO. El Niño is the phenomenon in which the sea water along the equator in the Pacific Ocean strongly heats up. This results in strong weather changes around the entire world. Typically El Niño increases rainfall totals and extremes in parts of South East Asia and islands in the western part of the northern Pacific Ocean and decreases rainfall totals and extremes in eastern Australia and Indonesia. The counter-phenomenon of El Niño is La Niña for which the effects are mostly reversed. La Niña is associated with temperature rises and increased heavy rainfall extremes in parts of Australia, particularly coastal regions in the north and east of the country.

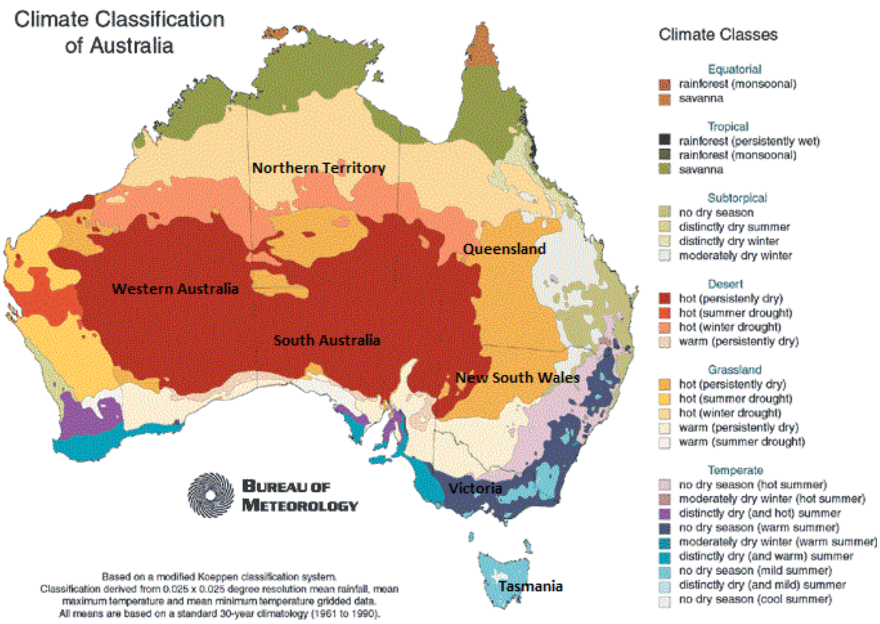

Figure 1-1: Map of Australia with climate classification (CSIRO, 2001)

The ENSO-phenomena is associated with many of Australia's natural hazards. El Niño events, accompanied by hot and dry weather conditions, can cause periods of drought lasting several months. La Niña typically produces heavier rainfall events, possibly causing periods of flooding in regions of Australia. Most memorable in recent history are the floods in Queensland during 2010-2011 (Van den Honert & McAneney, 2011).

Furthermore decadal and multi-decadal climate variability exists which affects the frequency and magnitude of ENSO-events. This phenomenon has two varieties: known as the Pacific Decadal Oscillation (PDO) and the Interdecadal Pacific Oscillation (IPO). Changes in climate due to IPO and PDO are related to sea surface temperature, just like ENSO. However the IPO events tend to last much longer: 20 to 30 years. Being strongly related with ENSO, IPO has heavy (multi-decadal) effects on flood risks in Australia.

Apart from climate variability, possible anthropogenic (human induced) climate change during the 21st century can potentially change the frequency and magnitude of flood events. Both climate variability and change strongly affect weather in Australia, leading to large-scale floods as have happened in Queensland during 2010-2011. Those floods have caused tremendous direct financial damage, estimated to be over 16 billion dollars. The total costs were estimated to be 30 billion dollars, including a 1% decrease of the Australian Gross domain product (Easdown, 2011). A research on flood risks associated to climate variability events like ENSO and IPO/PDO can be a helpful tool for the goals of control, constrain and prevention.

Since the effects of La Niña on flood events are the heaviest in the eastern parts of Australia, the research focuses on this region. By choosing this study area the research relates directly to the Queensland floods of 2010 and 2011. The specific states to be looked at are Queensland and New South Wales; both being prone by many flood events.

1.1 Aim of the project

The aim of this project is the evaluation of flood risks taking into account the uncertainties of climate variability modes. To accomplish this goal, different climate conditions are investigated, varying with climate states of the Interdecadal Pacific Oscillation/Pacific Decadal Oscillation and El Niño Southern Oscillation. It is expected that this project highlights uncertainties in common flood risk estimation.

1.2 Research questions

The full research question is as follows:

What is the impact of climate variability and change on the frequency and extent of floods in eastern Australia?

The research can be divided into the following sub topics:

Firstly a reference flood event is needed in order to be able to determine the deviations of other flood events. For that reason the 1 in 100 year flood event is calculated independent of any climate variability. This leads to the following sub question:

1. *What is the value of the 1 in 100 year flood independent of climate states for a selected catchment area in Eastern Australia?*

As this research focuses on the uncertainty due to climate variability the flood frequencies are to be calculated under different states of these climate variability modes. The flood frequencies are calculated with the data corresponding to either positive or negative phases (for instance El Niño and La Niña. This leads to the following sub questions:

2. *What are the conditional flood frequencies under different climate states?*
   - 5.1 *What are the conditional flood frequencies under IPO states?*
   - 5.2 *What are the conditional flood frequencies under PDO states?*
   - 5.3 *What are the conditional flood frequencies under ENSO states?*

Subsequently the influence of the climate variability modes on each other is investigated. It can be expected that flood frequencies will be altered if they are combined. To determine the quantitate effects the following question is answered:

3. *Does a combination of ENSO phases with IPO and PDO phases alter flood frequencies?*

With the created flood frequency curves the long-term uncertainty in flood frequencies can be estimated. Due to the variability of ENSO and IPO, with different flood frequencies deviate over a period of time. The goal is to estimate the uncertainty due to these climate variability modes:

4. *How does uncertainty in flood frequency estimates vary due to ENSO and IPO?*

A further interest is how these different flood frequencies translate into flood inundation. Firstly

5. *What is the extent of flood inundation under different climate states?*

   An additional question is the bandwidth of flood inundation extents for the uncertainty bounds calculated in sub question 4:

   5.1 *What are the uncertainty bounds of the extent of flood inundation under climate variability*

To be able to generalize the previously found results in the conditional flood frequency analyses to a broader scale, the Australian East coast, the spatial variance of the flood frequencies is investigated:

6. *Does spatial variance exist in the conditional flood frequencies?*

Finally the effect of possible anthropogenic climate change on flood frequencies and inundation is researched:

7. *To what extent could anthropogenic climate change influence flood frequencies and magnitudes?*

2 Theory

2.1 El Niño – Southern Oscillation (ENSO)

The El Niño-Southern Oscillation (ENSO) phenomenon has a big influence on the Australian climate. The phenomenon has two variations: El Niño and La Niña, whereas all in between is referred to as a neutral phase. El Niño is the state in which the sea water along the equator in the Pacific Ocean strongly heats up. This results in strong weather changes around the entire world (Royal Dutch Meteorological Insitute, n.d.). During La Niña events the effects are mostly reversed. The effects on Australia however have more impact (Bureau of Meteorology; Australian Government, 2014). In the eastern part the event is associated with heavier rainfall. This possibly results in floods across the entire east coast of Australia (Erik K. Veland, 2011). The most considerable flood event, presumably caused by a La Niña being one of the strongest ever recorded ENSO-events, occurred during 2010 and 2011 (Van den Honert & McAneney, 2011). The floods reached out across large parts of Queensland with an inundation area equivalent to the extension of France plus Germany. In 2011 the milder floods in Victoria and New South Wales intensified. Those events happened separately which provides an evidence of an underlying phenomenon: La Niña. Furthermore Wenju and Van Rensch (2012) have discovered a positive correlation between the strength of La Niña events (in terms of SOI; explained below) and South East Queensland (SEQ) rainfall, expectantly to increase flood risks. No correlation was found between El Niño strength and SEQ rainfall, suggesting El Niño events do not affect discharges and flood risks in this area.

An important feature of ENSO is the highly variable frequency and magnitude of the events. This variability is related to multi-decadal climate variability. To measure ENSO-phenomena a few indices and methods are available. The Southern Oscillation Index (SOI), the most basic index, measures the difference in sea-level atmospheric pressures between Tahiti and Darwin, Australia. (Kiem & Franks, 2001). Many indices, such as NINO3 and NINO4 are based on sea surface temperature (SST) data across the Pacific Ocean. Finally a Multivariate ENSO Index (MEI) can be used to indicate ENSO-events. It has been shown generally the MEI best reflects ENSO-events (Kiem & Franks, 2001) (Wolter & Timlin, 1998).

2.2 (Multi-) Decadal Pacific Oscillation IPO and PDO

The Interdecadal Pacific Oscillation is a multi-decadal variability in climate, both over the North and South Pacific. The frequency of phase changes is 15-30 years. Just like ENSO, IPO affects the sea surface temperatures and sea-level pressures at the Pacific Ocean. Those are mainly caused by shifts in circulation within the Pacific Ocean. The exact cause of IPO is still unknown, but it is confirmed to be related to the ENSO cycles; whether IPO exerts an effect on the ENSO cycle or ENSO variability changes the IPO is unclear though (Verdon & Franks, 2006). IPO has two phases: a negative and a positive phase. Three clear phases have been identified since 1920: two

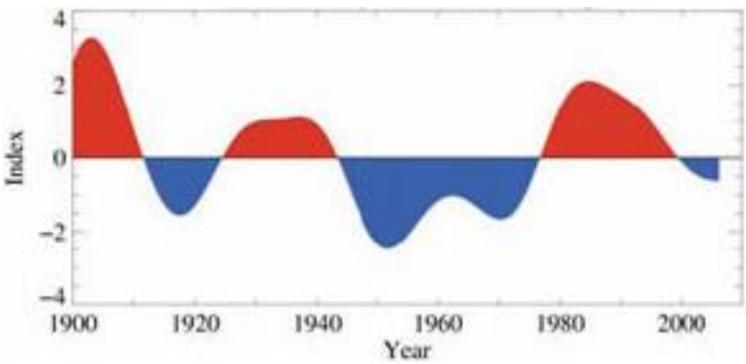

Figure 2-1: IPO Index (Ministry for the Environment New Zealand, n.d.)

positive phases (1920-1944 and 1978-1998) and a negative phase (1946-1976). These phases can be seen in Figure 2-1, which displays the IPO index.

The Pacific Decadal Oscillation (PDO) is strongly related to the IPO (Power, Casey, Folland, Colman, & Mehta, 1999) (Zhang & Church, 2012). The correlation of the two is said to be 0.96. The variation of the PDO in the north Pacific cause multi-decadal variability for the entire Pacific Ocean (IPCC, 2007). The effect though has high spatial variance; the PDO has a more significant influence on the Northern Hemisphere (Mantua N. , 2002), whereas the IPO has an effect on the whole Pacific Basin (Parker, et al., 2007) (Salinger, Renwick, & Mullan, 2001).

It has been proven that IPO may affect both the frequency and the magnitude of ENSO. (Kiem, Franks, & Kuczera, 2003). IPO negative phases are associated with an increased number of La Niña-events, therefore elevating flood risk.

2.3 Climate change

In recent decades there is a strong belief anthropogenic climate change exists. Just like anywhere in the world, Australia has to face the consequences of 'global warming'. Specifically for Australia the average temperature has risen by 0.9 °C in the last 100 years (CSIRO and Bureau of Meteorology, 2014), with the highest increase from 1970 onwards. Whereas annual total rainfall has increased nationally, it has decreased in South-eastern Australia though (Bureau of Meteorology; Australian Government, n.d.). Furthermore precipitation has become extremer globally, but it has decreased in the Eastern part of Australia since 1970 (Bureau of Meteorology; Australian Government, n.d.). If this trend of decreasing rainfall totals and peak intensities will persist, the flood risk will decrease. Another big threat to Australia is the global sea-level rising. Since 1880 the sea levels in the oceans have increased by approximately 225 mm. The sea-level rise in Eastern Australia is comparable to the global averages (CSIRO and Bureau of Meteorology, 2014).

Predictions for future climate changes are rarer for Australia compared to the high number of predictions for the Northern Hemisphere. This is mainly due to a lack of long-term datasets and thus trend-detection (Hughes, 2003). The predictions concerning the changes in (extreme) rainfall events have a high spatial variance. It is possible that the Eastern part of Australia will become drier with decreasing extreme events. In 1993, Whetton, et al. predicted the reduced rainfall extremes for Eastern Australia, which until now is the continuous trend (Bureau of Meteorology; Australian Government, n.d.). Murphy & Timbal (2008) argue that the trend of decreasing rainfall is due to regional climate changes, although these changes are a likely result of global climate change.

Many researches speak of a (or possible) El Niño-like global climate (Trenberth & Hoar, 1997) (Meehl & Washington, 1996) (Collins M. , 2005) (Timmermann, Oberhuber, Bacher, Esch, Latif , & Roeckner, 1999), expected to have a lower flood risk in Australia (2.1). It must be stated though a few of these researches are out-dated as the IPO was detected in 1999 (Power, et al.). Parker, et al. (2007) says that a full understanding of climate variability modes is needed to increase the accuracy of climate models used to study climate change. Philip (2009) has researched many climate models and concludes some are accurate enough to model climate change.

Contradictory to most studies mentioned before, Milly, et al. (2002) and Hughes (2003) conclude an increased flood risk for Eastern Australia due to extremer precipitation events. Remarkably CSIRO (2014), in addition to its report (CSIRO and Bureau of Meteorology, 2014), claims that natural variability is the main source of extreme rainfall magnitudes, with potentially a contribution by global warming. This contradicts to BOM data trends, which shows a decreasing trend in extreme rainfall events as mentioned before. CSIRO also states further research is needed to understand the effects of global warming on Australian rainfall.

The influence of the climate change on climate variability is still unclear. Collins, et al. (2010) speaks of the inability to assess the effect of climate change on ENSO activity, both in magnitude and frequency. On the other hand Philip (2009) says that the ENSO phenomena will remain unchanged in a climate with drastic changes in the mean state.

Unequivocally is the increased flood risk in the coastal areas due to sea-level rise (Department of the Environment; Australian Government, n.d.). The sea-level rise in Eastern Australia (CSIRO and Bureau of Meteorology, 2014), threatens the highly populated coastal areas with flooding.

2.4 Flood risks

Flood risk is a term which describes the probability of any flooding event occurring. The traditional and easiest concept for flood frequency estimation is the widely used exceedance chance method. This method is based on Annual Exceedance Probability (AEP) flooding. The percentage chosen for this is often 1%, which means a water height or discharge in a waterway or a rainfall quantity per time period which has the probability of occurring only once in every 100 years. The estimation of the 1% AEP flood is based on interpolation or extrapolation of a series of maximum values of different time periods. In Australia this concept is mainly used for quantitate analyses of flood risk.

When considering flood chances on top of exceedance chances, failure of water defence structures is also taken into account. Failure in this case means not only overflowing, but also other failure mechanisms such as erosion, piping and slip. The flood chance will obviously always be higher in comparison to the exceedance chance.

Flood risk is the most complex form of (probabilistic) flood risk assessment. It combines chances with the effect of the flood. The effect can be considered as only the flooded area, but can become more complex by introducing other risk aspects as damage (material/social) or exposure (number of inhabitants/buildings) and vulnerability (level of knowledge/strength of structures).

However in principle all methods are based on exceedance chance. An important assumption when calculating exceedance chances is a stationary situation over the entire period over which the calculation is applied. As stated multi-decadal climate variability exists, influencing rainfall patterns and totals. Therefore, for a certain moment in time the exceedance chance may differ from the long-term static mean value. This means that with varying periods of IPO and ENSO states, the flood risk can be over- or underestimated. Furthermore, possible (anthropogenic) climate change is also in contradiction with the assumption of a stationary situation.

3 Data

The study area for this research is the Upper Mary River Catchment in southern Queensland, Australia. The map of the catchment area is shown in Figure 3-1. Its size is approximately 985 km^2. The downstream end of the catchment is at Moy Pocket, where it flows into the main Mary River. The catchment is located in the coastal region of the Sunshine Coast. The catchment is characterized by its many creeks contributing to the flow of the river. The largest of these is the Obi Obi Creek, in which upstream a dam is situated; the Baroon Pocket dam, constructed in 1989. Kenilworth, the largest town in the floodplains of the river with its population of 300, lies at the confluence of the Obi Obi Creek and the Bellbird Creek, which is another name for the first segment of the Mary River.

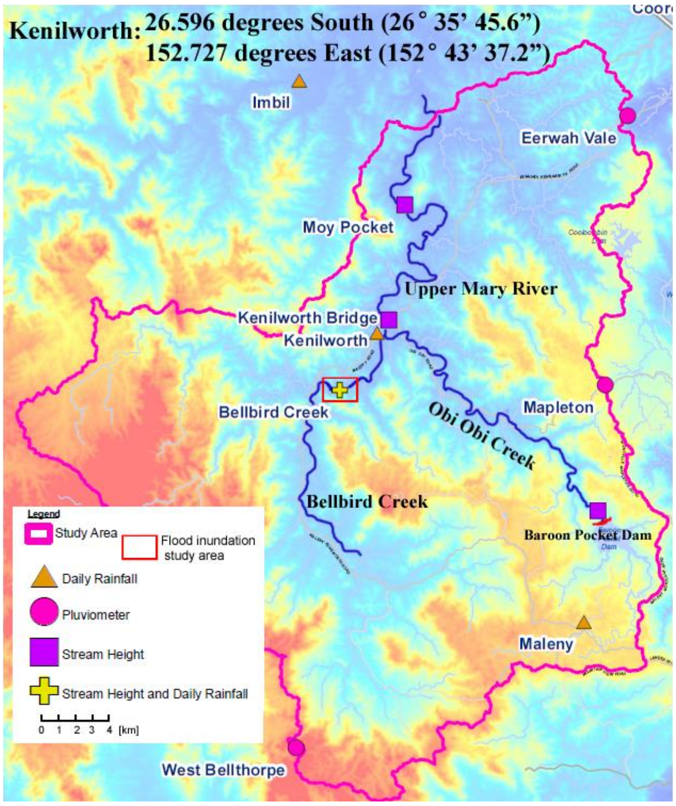

Figure 3-1: Map of Upper Mary river catchment (Smythe, 2014)

Stream heights in the Upper Mary River catchment have been recorded since 1920 near Kenilworth, with gauges at other locations since 1959, all operated by DERM (Department of Environment and Resource Management, Queensland). The catchment has the following major stream gauges of which the locations are shown in Figure 3-1:

Table 3-1: Stream gauges in the Upper Mary River catchment

Location	Length of data recording
Kenilworth	1926-1973
Obi Obi Creek	1920-1964
Bellbird Creek	1959-2011
Moy Pocket	1963-2011

With the finished construction of the Baroon Pocket dam in the Obi Obi Creek in 1989, the flood characteristics of the creek and all other downstream flows have changed. These include the streams at the locations of the gauges of both Kenilworth and Moy Pocket, making all pre-dam records for these three gauges inappropriate for a flood frequency analysis. The Bellbird Creek gauge thus has the longest appropriate time series of flow data. Because of the close distance of the Kenilworth and the Bellbird Creek gauges and the concurrent operation of those gauges, the data series of the Bellbird Creek can be extended back to 1926 (Smythe, 2014). This data extension is shown and explained in Appendix A: *Discharge data extension Bellbird Creek using Kenilworth gauge data.*

Figure 3-2 shows the bar-plot of all annual peak discharges including the extended series. The discharge peaks of 1932, 1939, 1940, 1942-1944 and 1957 are missing as there was found to be insufficient discharge data for the Kenilworth gauge for these years. This leaves a total number of 78 suitable discharge peaks.

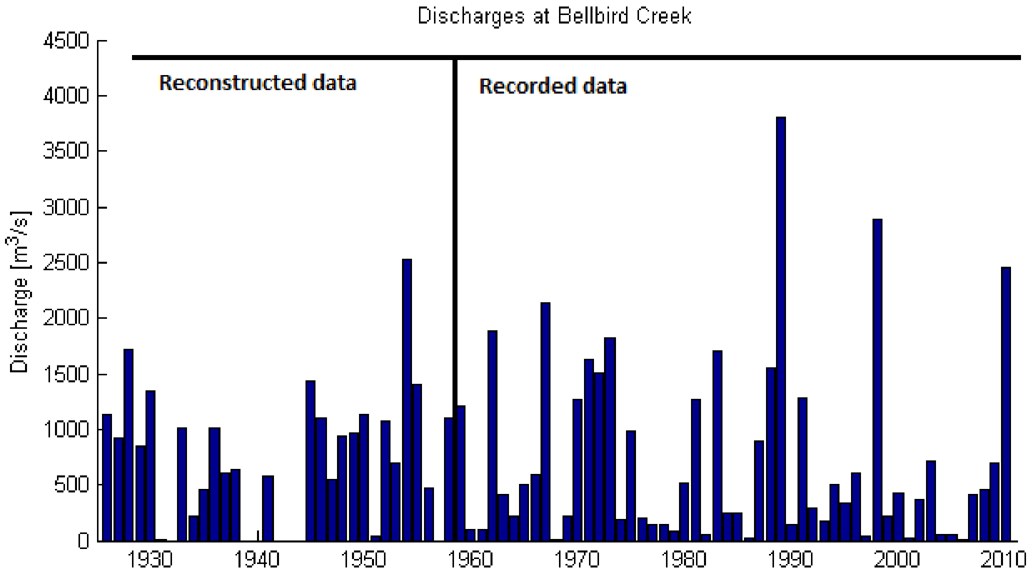

Figure 3-2: Discharges at Bellbird Creek

The flood inundation estimation is executed for an area in the Bellbird Creek, before the confluence of the Bellbird Creek with the Obi Obi Creek at Kenilworth. This rectangular area is marked in Figure 3-1. Figure 3-3 displays an aerial picture of the area. The elevation of the terrain around the gauge is available in a digital elevation map (DEM), displayed in Figure 3-4.

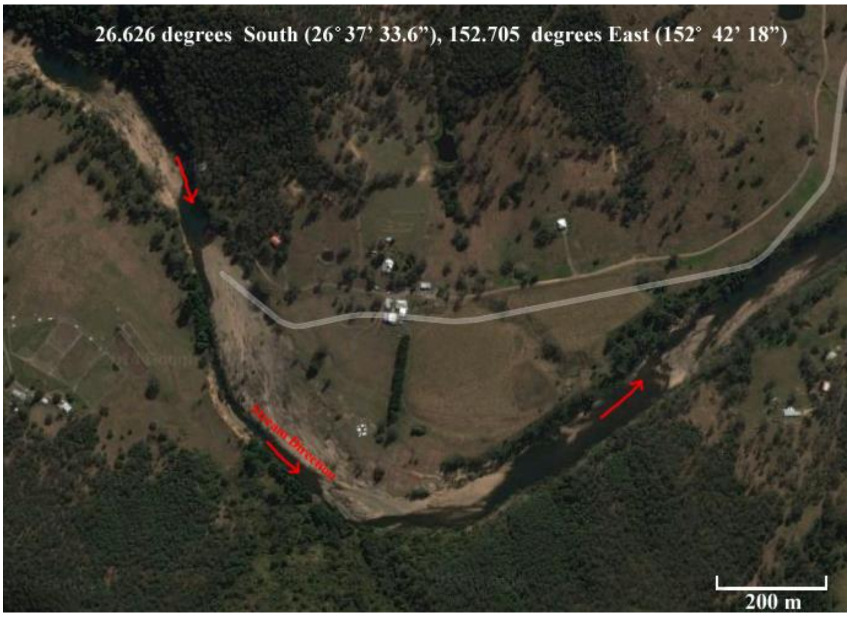

Figure 3-3: Aerial picture Bellbird Creek (Google, 2014)

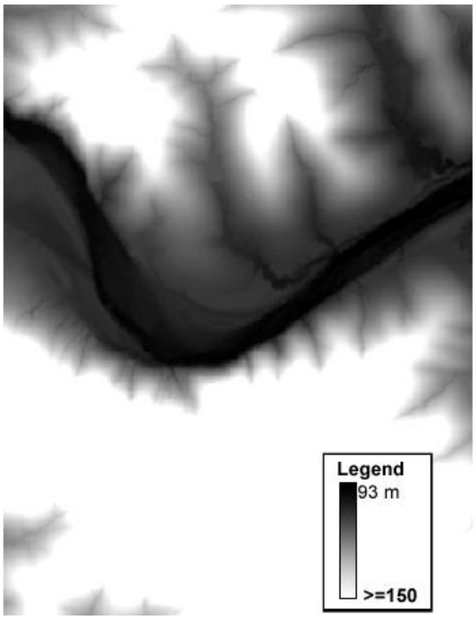

Figure 3-4: Digital elevation model

As can be seen in the two figures the main channel remains approximately the same width along this river segment with the stream direction from left to right. Upstream (facing downstream) the right floodplain is wider, with a high elevation area directly at the left bank of the channel. In the southern turn the right floodplain is narrowed down, whereas the left floodplain widens. At the most downstream end of the study area both floodplains widen, with presumably limited flow in the cove in the left floodplain.

4 Methods

4.1 Flood frequency analyses

A main focus of this research is the execution of flood frequency analyses. A distinction is made between unconditional and conditional flood frequency analyses. The unconditional flood frequency analysis is used as a reference for the remainder of the research. The unconditional analysis indicates the type of analysis in which all data is used, independent of the phases of the climate variability modes. This means the unconditional flood frequency curve is based on all 78 discharge peaks (see Chapter 3 for data). The conditional flood frequency is defined as the flood frequency that is valid for a single climate phase, for example during an El Niño year. To calculate the conditional flood frequencies the discharge peaks are selected which correspond to years of a certain climate variability phase, for example discharge peaks which occurred in years that are classified as El Niño are separated. The classification methods are described in 4.2. The global structure of the built Matlab-model, used to derive all flood frequency curves is described in Appendix C: *Flowchart of Matlab-model*.

4.1.1 Estimation of a flood frequency curve

Two methods exist through which flood frequencies can be estimated; either statistically with a record of gauged stream data or by developing a rainfall-runoff model. Normally the statistical method is the preferred method since it is the closest related to actual stream flows (NOAA Fishery Service, 2011). The basic idea behind the statistical method is that it relates annual peak discharges to recurrence interval (or exceedance chances). The result of the analysis is a flood frequency curve. For determining the curve many distribution models can be used to represent the relationship between the annual peaks and recurrence interval. Which model suits best is possibly different for every catchment area.

To create the frequency curve the first thing to do is to rank all annual peak discharges. The exceedance chance or recurrence interval of every ranked value is determined using the Weibull-equation ($T = n+1/rank$). All values can then be plotted.

At first, four different distribution models are tested for the full data range to find the best suiting distribution model for the catchment. Those four models are: Generalized Extreme Value (GEV), Gumbel (or Extreme value type 1), Log-Normal and Log-Pearson type III. After determining the best fitting model for this estimation only this model is used throughout the research.

The Lognormal, Gumbel and GEV distributions are fitted using the built-in functions of Matlab (lognfit and gevfit respectively). The Log Pearson type 3 requires more proceedings. The process of fitting this model is described in Appendix B: *Log-Pearson type 3 fitting*.

4.1.2 Determining the best fitting model

The best fitting model is determined by calculating Pearson's Coefficient of correlation (R^2), the Root Mean Square Error (RMSE) and the Index of Agreement (D) for each model, with the distribution having the highest values being the best fitting model. The 'Goodness of Fit'-parameters are calculated as follows (Biondi, et al., 2012):

$$R^2 = \left\{ \frac{\sum_{i=1}^{N} \left(\left(Discharge - \overline{Discharge} \right) * (y - \bar{y}) \right)}{\left[\sum_{i=1}^{N} \left(Discharge - \overline{Discharge} \right)^2 \right]^{0.5} * \left[\sum_{i=1}^{N} (y - \bar{y})^2 \right]^{0.5}} \right\}^2$$

$$RMSE = \left[\frac{1}{N} * \sum_{i=1}^{N} (y - Discharge)^2 \right]^{0.5}$$

$$D = 1 - \frac{\sum_{i=1}^{N} (y - Discharge)^2}{\sum_{i=1}^{N} \left(\left| y - \overline{Discharge} \right| + \left| Discharge - \overline{Discharge} \right|^2 \right)}$$

Discharge	=	Observed discharge data
$\overline{\text{Discharge}}$	=	Mean of observed discharge data
y	=	Model fit discharges
$\bar{y}$	=	Mean model fit discharges

4.1.3 Indicators of the presence of a climate variability mode

The first indicator of climate variability (IPO, PDO and/or ENSO) having an effect on the flood frequencies is the separation of the flood frequency curves of the positive and the negative phases. The separation is made visible by plotting the two curves.

The separation of the flood frequency curves can also be expressed numerically by testing the independency of the curves through a student's t-test. This two-sampled test calculates the significance of the independency. The t-test is based on the following equation:

$$t = \frac{\bar{x} - \bar{y}}{\sqrt{\frac{(n-1)s_x^2 + (m-1)s_y^2}{n+m-2}}}$$

$\bar{x}$ & $\bar{y}$	=	Sample means
s_x & s_y	=	Sample standard deviations
n & m	=	Sample sizes

The p-value, the probability the means of the samples are equal, of the samples can be determined using the t-value and the degrees of freedom (n+m-2). A low p-value indicates more significant differences between the samples.

Another evident indication of a climate variability signal is the strength of the signal, expressed by the 100 year flood event (a flood event with a return time of 100 years or an annual exceedance probability of 1%) of the negative phase divided by the 100 year flood event of the positive phase (e.g. La Niña/El Niño). The 100 year flood events can be derived directly from the corresponding flood frequency curves.

4.2 Identification of climate variability phases

As mentioned in 4.1 the full discharge data set is divided into sets which correspond to the climate phases. To select the peaks that have occurred during a certain climate variability phase, the phases must first be identified. The classification method for the IPO is described in 4.2.1, in 4.2.2 for the PDO and in 4.2.3 for the ENSO.

4.2.1 Interdecadal Pacific Oscillation (IPO)

The following IPO states have been distinguished since 1920 (see Chapter 2.2):

- IPO positive (1) 1920 – 1944
- IPO negative 1946 – 1976
- IPO positive (2) 1978 – 1998

The current phase of the IPO is a topic of debate. Due to its very low frequency signs of an IPO state change will be evident after a long amount of time. The smoothing of Sea Surface temperature data, through which the IPO index is derived, is done with time durations of up to 30 years, making it hard to say what the current state is. It can be stated though that the La Niña events of 2010 and 2011 occurred in an IPO negative phase. The first reason is the strong negative values of the PDO index derived by Mantua (2014), confirmed by the US National Climatic Data Center (NCDC; n.d.). Due to its strong correlation to the IPO (see 2.2), 2010 and 2011 values can be used for the IPO negative phase. Wenju & Van Rensch (2012) have detected three further signs of an IPO state change for the 2011 event: large rainfall anomalies and SOI values, a significant ENSO-rainfall relationship and a global circulation state, all unique for or similar to previous IPO negative phases.

For the uncertainty analysis, which is described in 4.3 a longer record of IPO phases is required. To classify IPO phases prior to 1920 the IPO reconstruction of Verdon & Franks (2006) is used. They have bundled several IPO reconstructions into one composite IPO index. This composite index shows clear phase switches over the past 400 years.

4.2.2 Pacific Decadal Oscillation (PDO)

To determine the phases of the PDO the monthly data series of Mantua (2014) is used. As becomes evident from this data, the phases of the PDO are less distinct than the IPO's, as the variation in the values is not filtered by smoothing the raw data. For this reason a neutral phase is added besides the positive and negative phases.

The yearly value of the PDO index is determined by a 12 month running average. It has been chosen to use the hydrological year, similar to the hydrological year for which the discharge peaks have been derived (see Chapter 3), running from October to September. Any year for which the 12 month average value of the PDO index exceeds the threshold of 0.5 standard deviation is classified as a PDO positive year and an average below 0.5 standard deviation as a PDO negative year. Any year for which the average lies between 0.5 and -0.5 standard deviation is considered a neutral year.

4.2.3 El Niño – Southern Oscillation (ENSO)

Many methods exist by which ENSO events can be identified. As stated before (2.1), multiple indices exist that describe the strength of an ENSO event. Kiem & Franks (2001) state that the MEI is the most robust index out of the three types (SOI and SST-based are the other indices). They state this holds for other catchments in Eastern Australia, although local variability may exist. For this research a quick analysis is done using different methods and indices. The following indices are tested:

1. Multivariate ENSO index (MEI) (Wolter K. , 2011)

2. NINO 3.4 index, Hadley Centre Sea Ice and Sea Surface Temperature (2014) for raw data & US NCAR's Climate Analysis Section (2008) for normalized data
3. Southern Oscillation Index (SOI) (Australia's BOM Climate Analysis Section, 2014)

The following methods are tested for every index:
- Three month average, November - January
- Six month average, October - March
- Twelve month average, April – March

El Niño (La Niña) events are defined as any year in which the average index value is above 0.5 (below -0.5) for the MEI and NINO 3.4 and below -5 (above 5) for the SOI (Kiem & Franks, 2001). A condition for this is a normalized table of values (with average 0 and standard deviation 1 (10 for SOI). In any other case El Niño is defined by the average anomaly exceeding 0.5 standard deviation.

The ENSO reconstruction is obtained via Mann (Mann, Bradley, & Hughes, 2000). This reconstruction is used for the uncertainty analysis (see 4.3). Mann has reconstructed the ENSO activity back to 1649. The thresholds to define the positive (El Niño), neutral and negative (La Niña) events are similar to the ones used in this research: 0.5 and -0.5 standard deviation.

4.3 Analysis of the uncertainty due to climate variability

The general method is to estimate the 100 year flood and its uncertainty as a function of different data lengths. The leading methodology is Franks (2014). From the ENSO and IPO reconstructions (see 4.2.1 and 4.2.3) a random time period is chosen starting with a length of 20 years. Using the associated flood frequency curve for a specific state of the climate variability mode (e.g. the El Niño flood frequency curve) a random flood event can be generated per year. If done for the entire time period of 20 years a flood distribution is created. This distribution is fitted to a Log-Pearson type 3 distribution. Using that fit the 100 year flood event can be calculated. Repeating these calculations in a Monte Carlo simulation a series of 100 year flood events is created. The variety in this series represents the uncertainty of the 100 year flood estimation. The 95% confidence interval is constructed by a basic bootstrap method of creating the lines in which the sorted values from 2.5% to 97.5% lie in between.

Subsequently, a longer data length can be used, from which another distribution of 100 year flood events is obtained. By performing similar simulations for multiple data lengths the uncertainty in 100 year flood estimations can be assessed by comparing the 95% confidence intervals of the distributions.

This method is summarized in Figure 4-1, when only taking into account the uncertainties of ENSO events. For IPO the same method holds, but the neutral events are left out.

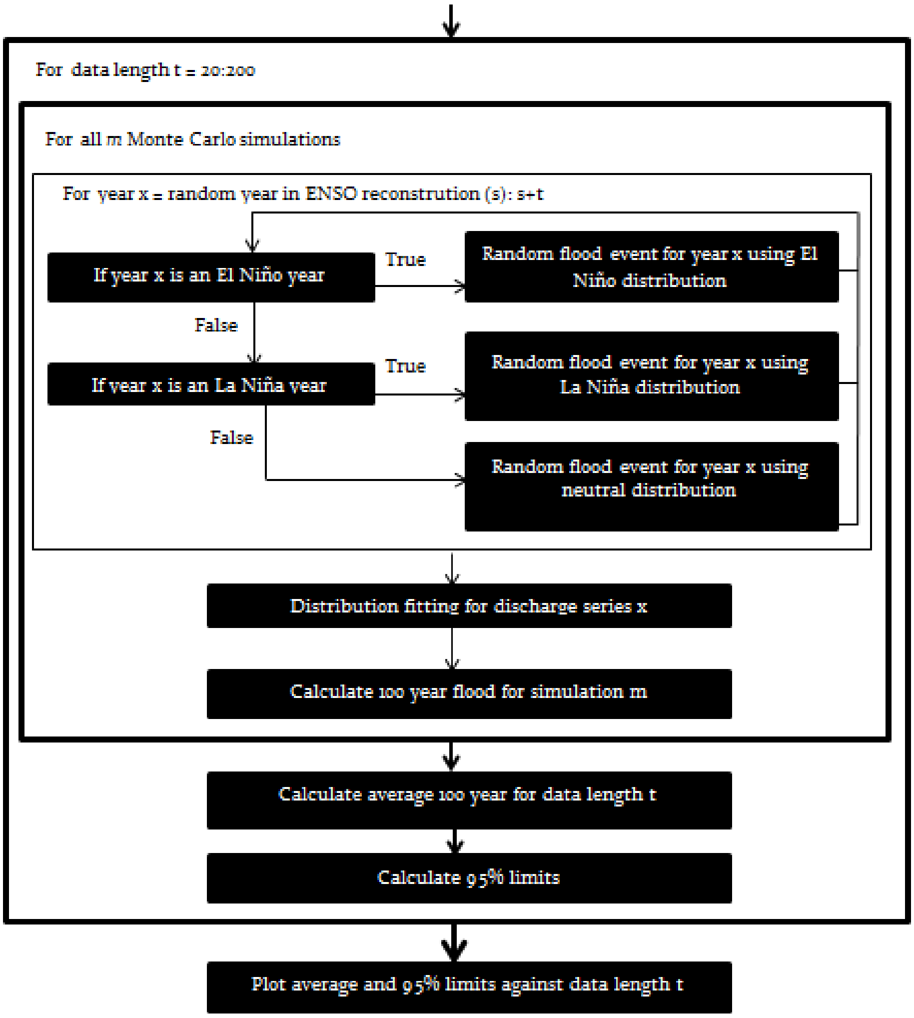

Figure 4-1: Flowchart of uncertainty estimation

4.4 Flood inundation modelling

To estimate the extents of flood inundation a flood plain mapping analysis is executed using HEC-RAS. HEC-RAS is a one-dimension modelling software package, with a few possibilities to extend to a basic two-dimensional analysis. When modelling in one dimension, one is only considering the direction of the stream. This implies a uniform stream velocity pattern along the cross-section of the flow, which in reality could never exist. Especially when (wide) flood plains are involved a one-dimensional model can be in great error.

The main input for HEC-RAS is the geography of the area. The geography of the Upper Mary River is available in an ArcGIS-compatible GRID-format. To import the geography to HEC-RAS the geographic data must be transformed into river geometry using an ArcGIS-extension called HEC-GeoRAS. The description of how the river bathymetry was created can be found in Appendix D: *Description of ArcGIS-model.*

After importing the bathymetry in HEC-RAS the Manning's n coefficient for roughness must be assigned for the flood plains and the channel. It is assumed that the coefficient is constant for every cross-section. Assuming this simplifies the model, but introduces a source of error. The first estimation of the n coefficient is made using the aerial photo of the terrain, previously shown in Figure 3-3. Using the Manning's n table (Arcement Jr. & Schneider, 1984), the following values have been chosen for the n coefficient: 0.04 for the river channel, indicating a clean but uneven terrain and 0.06 and 0.1 for the left and right bank indicating light and dense vegetation respectively.

Next, the steady flow details must be defined through boundary conditions. Steady flow analysis was chose over unsteady flow analysis because the only available data is static discharges. The initial conditions of the steady flow analysis are the discharge values corresponding to the 1 in 100 year conditional flood magnitudes. Secondly the external boundary condition is set as a normal depth value, for which the water slope is a good estimation (Brunner & Gee, 2005). The boundary condition is initially set to 0.001 normal depth at the downstream cross-section. (Merwade, 2012).

HEC-RAS simulates the water height in a steady flow analysis using the geographical data and the steady flow conditions. It is assumed the entire flow occurs in a subcritical flow regime. Subsequently the model must be calibrated using rating curves (Discharge – water height relationship), which is available through BOM (Bureau of Meteorology, Australia) and DERM (Department of Environment and Resource Management, Queensland) data (Smythe, 2014). The model is calibrated using the previously defined normal depth boundary condition.

4.5 Climate Change

It has become apparent from the literature study that no consensus exists on what the effects of climate change are on the frequency and magnitude of heavy rainfall events (2.3). Therefore no precise quantitate predictions can be made for the flood frequency and inundation events in the Upper Mary River catchment. The variety of future changes according to multiple researches can be tested though, expected to show a range of possible effects on the catchment area. Below the researches are listed of which the predictions are tested. These researches were chosen as they had a quantitative future prediction.

- The Queensland government proposed to incorporate a 5 per cent increase of extreme rainfall intensity per degree of global warming. Considering the projected 2°C increase by 2050 a total increase of 10 per cent in intensity is realistic. (State of Queensland, 2010). For the purpose of this research a similar increase in extreme flood discharges is assumed, which itself is a false assumption but it can show a possible degree of increased flood risk.
- Walsh, et al. (2001) modelled extreme rainfall events on the basis of the IPCC's (Intergovernmental Panel on Climate Change) Third Assessment Report (*Climate Change,* 2001). More recent interpretations of IPCC's reports are not available. Walsh, et al. has scaled the global IPCC report down to South-East Queensland, reducing the uncertainty of the conclusions drawn from the global report. They predicted a decrease of the 40 year return time daily extreme rainfall event to an 18 year return time event by 2050. Assumed is a strong correlation between daily extreme rainfall return times and flood event return times.
- Milly, Wetherald , Dunne, & Delworth (2002) modelled a decrease of the return time of the 100 year flood magnitude to a 30 to 40 year flood event by 2050 for a large catchment area in Eastern Australia (Northern New South Wales and Southern Queensland). Although dated this is the only of the selected research that expresses the climate change directly in terms of flood events.

5 Results

5.1 Flood frequency analyses

5.1.1 Best fitting distribution model

Four probability distribution models are fitted to all (unconditional) discharge data: Generalized Extreme Value (GEV), Gumbel, Lognormal and Log-Pearson type 3 (LP3) (see 4.1.1). The model fits are shown in Figure 5-1.

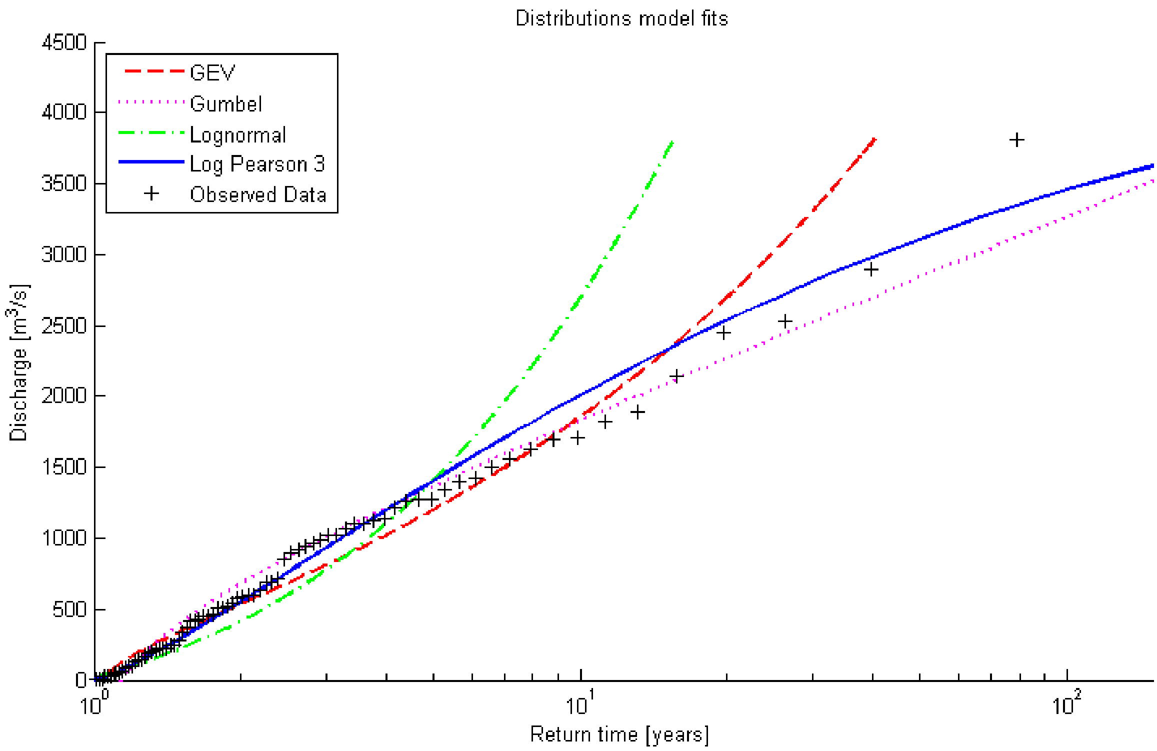

Figure 5-1: Distribution model fits

Both the Gumbel (Extreme value type 1) and the Log-Pearson type 3 distribution models have good graphical fits. This also becomes apparent from the 'goodness of fit'-parameters Pearson's Coefficient of Determination, Root Mean Square Error and the Index of Agreement (see 4.1.2). The values of these parameters are shown in Table 5-1.

Table 5-1: Goodness of fit parameters

	Coefficient of Determination R^2	Root mean square error (RMSE)	Index of agreement (D)
Lognormal	0.847	1088	0.797
LP3	0.983	109.1	0.995
GEV	0.953	225.6	0.981
Gumbel (EV1)	0.967	135.0	0.991

According to U.S. Water Advisory Committee on Water Data (1982) Log-Pearson type 3 is the recommended flood frequency analysis method and considering the LP3 having the best fit for this data set, this distribution model is used for the flood frequency analyses.

5.1.2 Unconditional flood frequency analysis

Figure 5-2 shows the LP3 fit including its 95% confidence interval. The corresponding values can be found in Table 5-2.

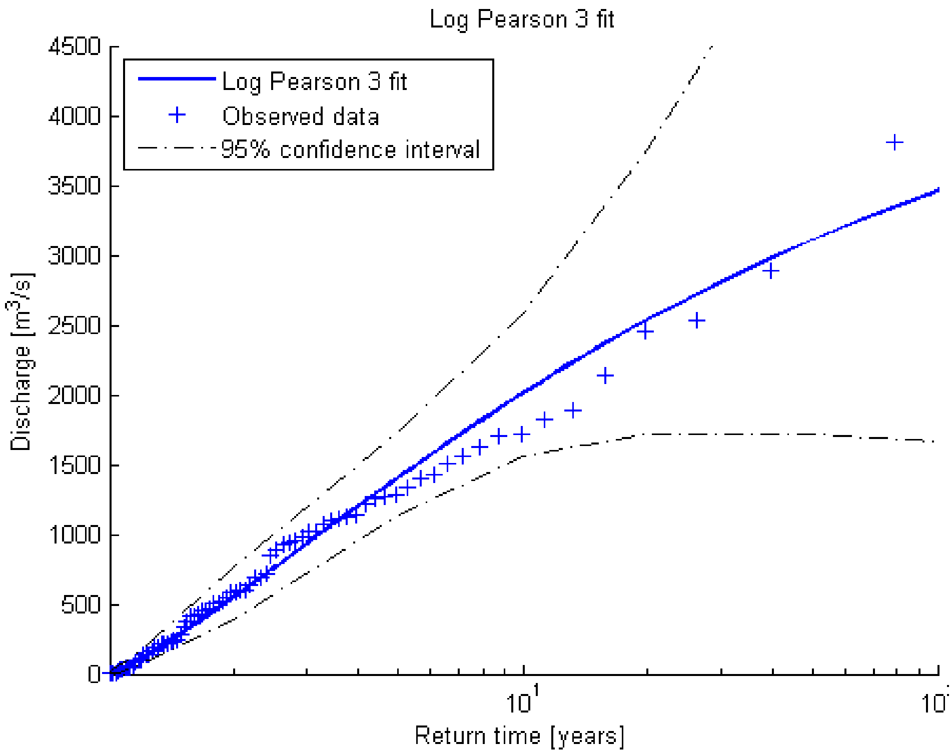

Figure 5-2: Log-Pearson type 3 fit and 95% confidence interval

Table 5-2: Flood frequency table

Return time [years]	Expected discharge [m³/s]	Lower 95% confidence limit [m³/s]	Upper 95% confidence limit [m³/s]
2	546	391	764
5	1405	1143	1727
10	2008	1560	2583
20	2536	1713	3755
50	3112	1718	5637
100	3459	1659	7215

The uncertainty in the modelled flood frequency curve is relatively small for return times up to ten years. For higher return times the uncertainty grows rapidly due to a lower amount of data points in this range. Despite of the high uncertainty, the fitted model seems valid as there are no major outliers which affect the model fit. The expected 100 year flood event of 3459 m^3/s can therefore be used as a reference to the conditional flood events of the climate variability modes. For every conclusion from this flood frequency curve the uncertainty and the assumption the model fit is correct must be kept in mind though.

5.1.3 Conditional flood frequency analyses

The following subparagraphs provide the results of the conditional flood frequency analyses. Subparagraph 5.1.3.1 shows the IPO flood frequencies, 5.1.3.2 the PDO flood frequencies and 5.1.3.3 shows the ENSO flood frequencies. Finally 0 provides an overview of the 100 year floods under the different climate variability modes and states.

The years and their identified climate states according to the classification methods (4.2) for all climate variability modes can be found in Appendix E: *List of years and corresponding climate states.* The plots of the observed discharge data for the classified years are displayed in Appendix F: *Stratified observed discharge data according to identified climate states*. Finally Appendix G (*Tabulated values of unconditional and conditional flood frequency curves*) provides the values corresponding to the fitted flood frequency curves and their 95% confidence intervals.

5.1.3.1 IPO flood frequencies

The full discharge data set, consisting of 78 discharge peaks (see 3 and 4.1.1), is divided into two sets of peaks that have occurred in positive or negative IPO years. The classification of the IPO years is described in 4.2.1 and the IPO positive and negative years have been listed in Appendix D. The divided peaks are plotted using the Weibull method (see 4.1.1). These plotted sets can be seen in Appendix F and are also visible in Figure 5-3 (observed data). Figure 5-3 also displays the fitted conditional flood frequency curves for the positive and the negative state of the IPO and its 95% confidence intervals. The values corresponding to the plotted lines are tabulated in Appendix G: *Tabulated values of unconditional and conditional flood frequency curves*, along with the values of the unconditional flood frequency curve (5.1.2)

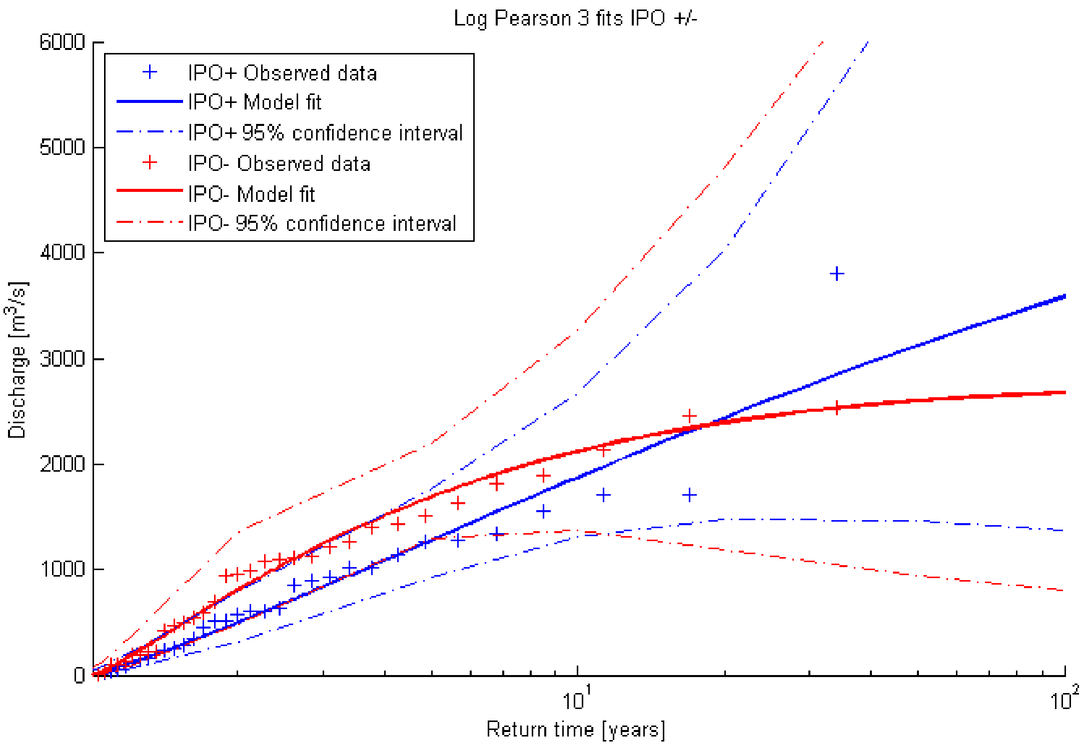

Figure 5-3: IPO positive and negative model fits

Whereas it can be expected the negative IPO phase yielding a higher or equal flood frequency curve (2.2), a higher positive IPO phase flood event (for a return time of 100 years) is unexpected. Furthermore the 100 year flood for the IPO negative phase is lower than the unconditional 100 year flood event and the IPO positive phase's is higher than the unconditional 100 year event. A reversed effect was expected as the negative IPO state is associated with heavier rainfall events and an increased number of La Niña events as stated in 2.2.

For a return time up to ten years the results seem more logical, with the negative IPO phase returning a higher flood event at the same return time compared to the positive IPO phase. Also the 95% confidence interval bounds are higher for the negative IPO phase, also indicating a higher chance of a flood event with a higher discharge occurring in an IPO negative phase opposed to the positive phase. For flood events with a return time of over eight years the uncertainty bounds of the negative IPO phase widens stronger than the positive IPO's. This strong widening of the uncertainty bounds indicates a higher variance in the observed extreme flood events, whereby the estimation of the flood frequency curve becomes more uncertain. The expected 100 year flood event in IPO negative phases is therefore highly uncertain.

Furthermore the positive IPO phase fit suffers from two high outliers as can be seen in Figure 5-3. There is no reason to rule these two out on the lack of independency, since they occurred in 1989 and 1998; the assumption of independency being required for a flood frequency (2.4). The 1998 peak though is the last year of the positive IPO phase (2.2), which inclines that this peak may have occurred in a changing climate. Ruling out this single peak changes the resulting 100 year floods, but does not result in a reversed IPO strength (negative being higher than positive, see 4.1.3), with 100 year floods of 3585.5 and 2674.6 m^3/s for the positive and the negative phase respectively. The plots of the flood frequency curves in which the peak was ruled out can be seen in Appendix H (*IPO flood frequency curves without 1998 peak*).

A further proof of the weak IPO signal is the P-value of the data (4.1.3), being 0.475, suggesting a reasonable chance the means of the data sets are equal. Because the P-value is independent of the model fit, this indicates a weak IPO signal in the data itself. If the 1998 peak is removed from the data the P-value decreases to 0.27, but it still does not show a strong IPO signal.

5.1.3.2 PDO flood frequencies

Just like for the IPO, the data has been split into the negative and positive phases, but this time adding a neutral phase (4.2.2). Figure 5-4 on the next page displays the fitted Log-Pearson 3 distributions for the positive and the negative state.

Whereas the IPO does not have a clear signal, the PDO does as becomes apparent from the indicators (4.1.3). Firstly a clear graphical distinction can be seen in Figure 5-4 between the two model fits and its confidence intervals. Secondly the 100 year flood events for the positive and negative state are 3010.6 and 5008.9 m^3/s respectively, which results in a PDO strength of 1.66 for a 100 year flood (negative divided by positive PDO). The p-value of 0.0068 gives further evidence of the distinct results of the two phases. These results are noteworthy, considering the weak IPO signal concluded in the previous paragraph. Whereas the IPO and the PDO normally have a strong correlation (see Chapter 2.2), this correlation is not evident for the Upper Mary river catchment area. Furthermore it could be expected the PDO would have the weaker signal in oppose to the IPO, as the PDO strength weakens further south (again see Chapter 2.2).

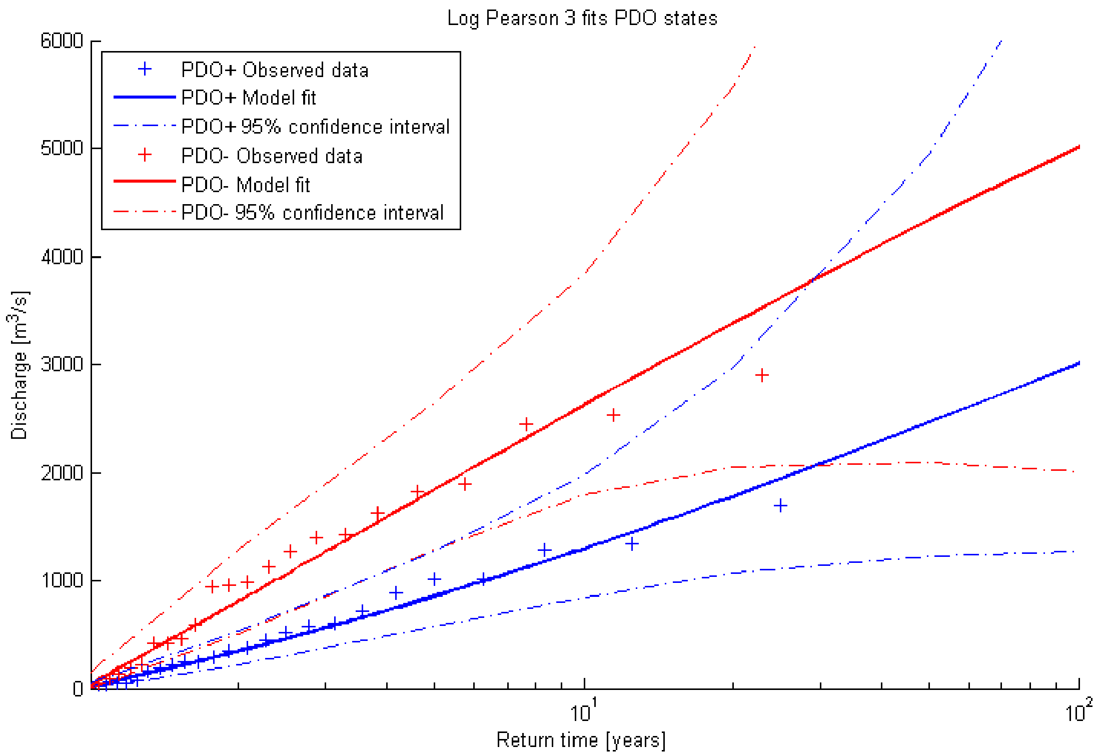

Figure 5-4: PDO positive and negative model fits and confidence intervals

5.1.3.3 *ENSO flood frequencies*

As explained in 4.2.3 many methods and indices exist by which ENSO events can be identified. Through these methods and indices nine different lists of ENSO events (three methods combined with three indices) have been identified. An analysis of these events has led to the values in Table 5-3. The observed discharge data corresponding to the distinguished ENSO years for the three indices (with a six month average) can be found in Appendix F: *Stratified observed discharge data according to identified climate states.*

Table 5-3: ENSO index and method analysis

	NINO 3.4			MEI			SOI		
X month average:	3	6	12	3	6	12	3	6	12
El Niño 100y flood	3278.2	3938.1	3358.9	3165.8	3439.5	4438.2	3576.6	4518.6	3197.9
La Niña 100y flood	4612.8	4811.9	4775.5	5101.8	5179.2	4322.5	3779.9	3813.2	5029
ENSO strength (La Niña/El Niño)	1.41	1.22	1.42	1.61	1.51	0.97	1.06	0.84	1.57
P – value	0.0015	0.0009	0.0021	0.0023	0.0018	0.0038	0.0027	0.0018	0.0021

The table shows the NINO3.4 index wields the lowest p-values, marking a more significant difference in means of the El Niño and La Niña phases' discharges. Whereas using the MEI lead to the lowest p-values in Kiem's and Franks' research on the identification of ENSO states (2001), the MEI results in slightly higher p-values for the Upper Mary River catchment area. This indicates the MEI indeed is not always the better identification index as stated by Kiem and Franks. Contradictory, using the MEI wields a higher ENSO strength (100 year event of La Niña divided by El Niño's 100 year event) for the method of a three or six month running average. In this research the focus lies on extreme flood events and for that reason the MEI is chosen to be the identification index as the ENSO strength is the highest. As the six month running average wields the lowest p-value and a reasonably high ENSO strength, this method is most preferred to define ENSO events.

By fitting the (positive) El Niño and (negative) La Niña to a Log-Pearson type 3 distribution Figure 5-5 is created.

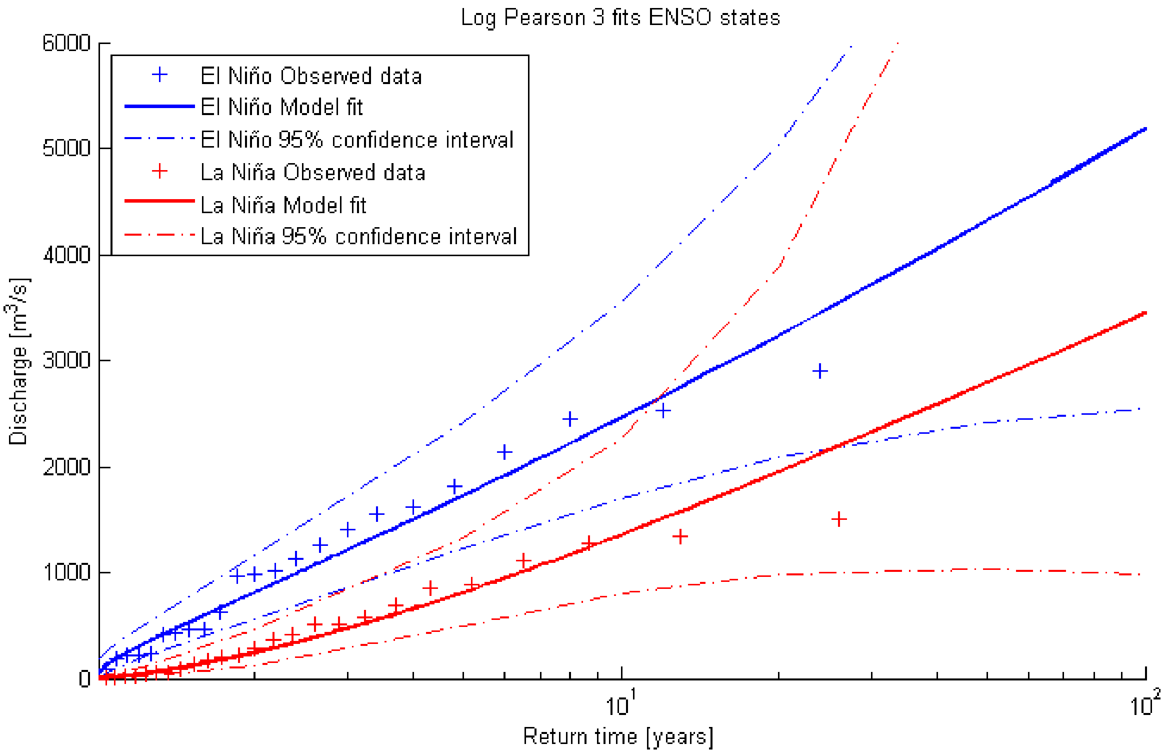

Figure 5-5: ENSO positive (El Niño) and negative (La Niña) model fits

It can be seen that El Niño events do not change the flood frequencies of this catchment significantly, confirming the low correlation between South East Queensland rainfall and El Niño events found by Wenju and Van Rensch (2012; see 2.1). But because of the higher flood frequencies associated with La Niña events a signal is visible in the fitted data. The 100 year flood events for the El Niño and La Niña events are 3439.5 and 5179.2 m^3/s respectively, wielding an ENSO strength of 1.51. This, along with the low p-value of 0.0018, gives evidence of the Upper Mary River catchment being sensible to both short-term variability from ENSO (three to seven years) and longer term variability (PDO). As can be seen in Appendix D, many years of the data set do not have similar PDO and ENSO states at the same time, suggesting an independency of the results for the two phases, giving further prove of the strong signals as the divided observed data (into the positive and negative phases) for the two climate variability states are different.

5.1.3.4 *Overview conditional flood magnitudes*

Table 5-4 gives an overview of the different flood magnitudes corresponding to the 1% Annual Exceedance Probability (100 year flood). Tabulated values for events with other return times can be found in Appendix G: *Tabulated values of unconditional and conditional flood frequency curves*. The values of the upper and lower confidence limits are also tabulated in this appendix.

Table 5-4: Overview 100 year floods

	100 year flood [m³/s]	Percentage of deviation compared to unconditional flood frequencies
Unconditional	3459.3	
IPO positive	4068.0	+17.6 %
IPO negative	2674.6	- 22.7 %
PDO positive	3010.6	- 13.0 %
PDO negative	5008.9	+44.8 %
ENSO positive (El Niño)	3439.5	-0.6 %
ENSO negative (La Niña)	5179.2	+49.7 %

5.1.4 Flood frequencies for combinations of PDO and IPO with ENSO

One possible characteristic of the IPO and the PDO is changing the frequency of ENSO events (2.2). In Table 5-5 the frequencies of occurrences of combined events are given. The years in which these combined events have occurred can be found in Appendix E: *List of years and corresponding climate states.*

Table 5-5: Frequencies of combined climate variability modes

	Positive IPO	Negative IPO	Positive PDO	Neutral PDO	Negative PDO
El Niño	12	9	13	10	2
Neutral	17	10	9	16	5
La Niña	5	14	2	6	15
Total	34	33	24	32	22

As becomes evident from the table the negative IPO state increases the frequency of La Niña events and decreases the number of El Niño and neutral events, proven to be one of the characteristics of the IPO (see 2.2 for references). Judging from the frequencies only it could be expected that the negative IPO phase strongly increases the flood risk as the number of La Niña events increases, but this did not become evident in the IPO conditional flood frequency analysis (Paragraph 5.1.3.1).

The phase of the PDO also has a correlation with the ENSO events. As can be seen in Table 5-5 the combined events with the same state (PDO+/El Niño, ENSO and PDO neutral and PDO-/La Niña) have the highest frequencies.

Another characteristic of the IPO and PDO is increasing the ENSO strength during the negative phases (2.2). To analyse this feature for the Upper Mary River the following division is made:

- La Niña years in a negative IPO phase
- La Niña years in a positive or unknown IPO phase (1999-2009)

Only La Niña is considered to be relevant, as El Niño does not have a big influence on flood frequencies (see 5.1.3.3). Figure 5-6 shows the fitted distributions for the discharges that have been divided into the categories. Subsequently Figure 5-7 shows the fitted models for the same categories but with the PDO instead of the IPO.

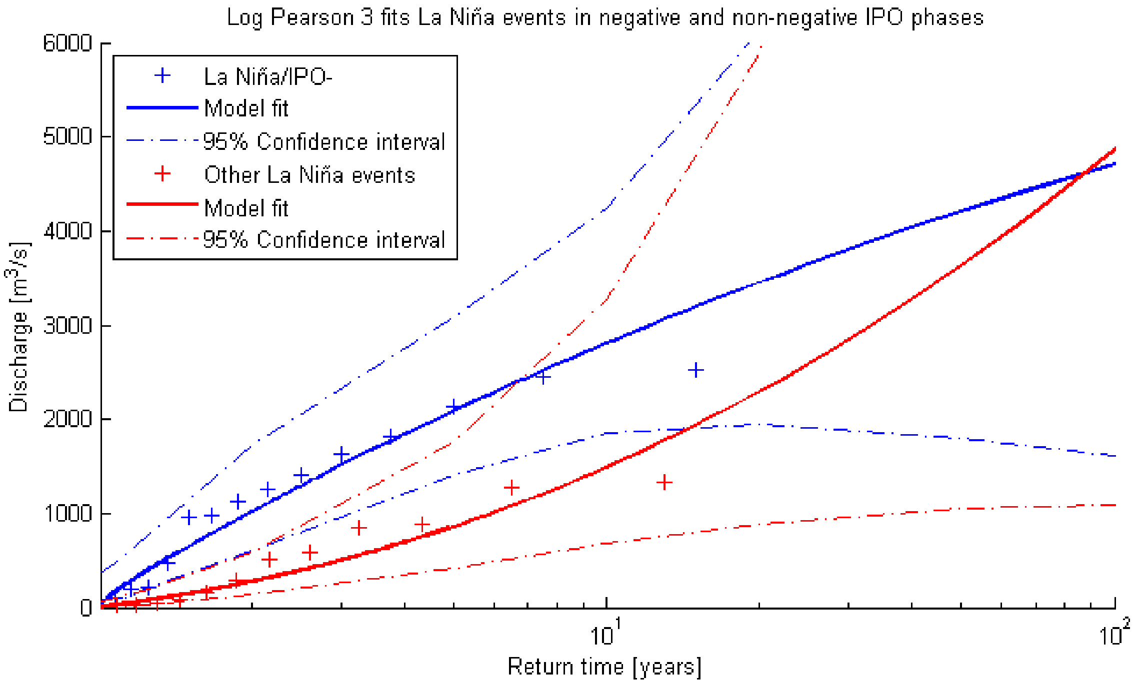

Figure 5-6: Combined IPO and ENSO flood frequencies

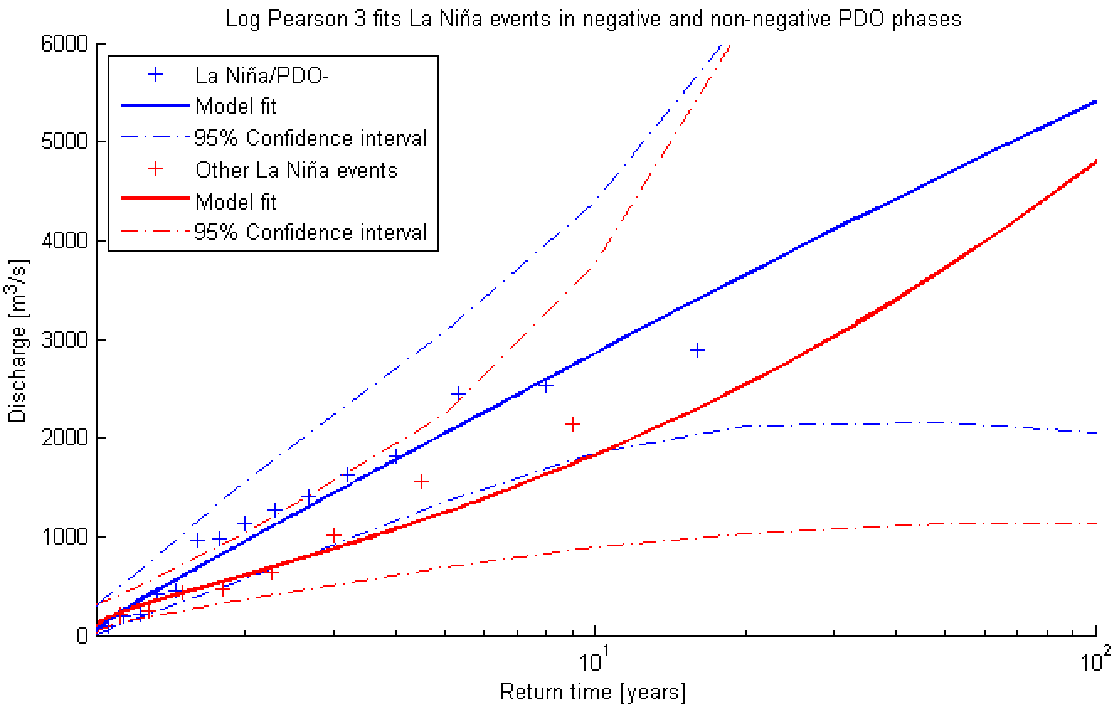

Figure 5-7: Combined PDO and ENSO flood frequencies

Both the combinations of IPO and the PDO states with La Niña events (Figure 5-6 and Figure 5-7) show a certain degree of separation. Typically La Niña events occurring in negative IPO or PDO phases have an increased flood frequency. It can be seen that the IPO compared to the PDO has a stronger effect on La Niña flood frequencies, although this is not expressed through the 100 year floods which are almost equal. The 100 year floods are not representative though, since there are few data points to correctly model the flood frequency curve for higher return times.

The p-values provide a numerical significance for the separations of the flood frequency curves. The p-value of the division on the base of the IPO phases is 0.013 and 0.299 for the PDO. This gives significant proof for the increased La Niña impact on discharge peaks during a negative IPO phase.

Concluding from Table 5-5 it can be said that the PDO and the IPO both change the frequencies of the ENSO events and via Figure 5-6 it becomes evident the negative IPO phase increases the flood magnitudes of La Niña events.

5.2 Uncertainty in flood frequency estimates

To assess the uncertainty due to climate variability this uncertainty was executed. The methods are explained in Chapter 4.3. Figure 5-8 displays the results of this uncertainty analysis: the average 100 year flood event and its 95 and 80 % confidence intervals for data lengths in the range of 20 to 200 years. The considered variable climate state is the ENSO since it has a stronger signal in the Upper Mary River catchment compared to the IPO (see results in 5.1.3). The used ENSO reconstruction is described in 4.2.3.

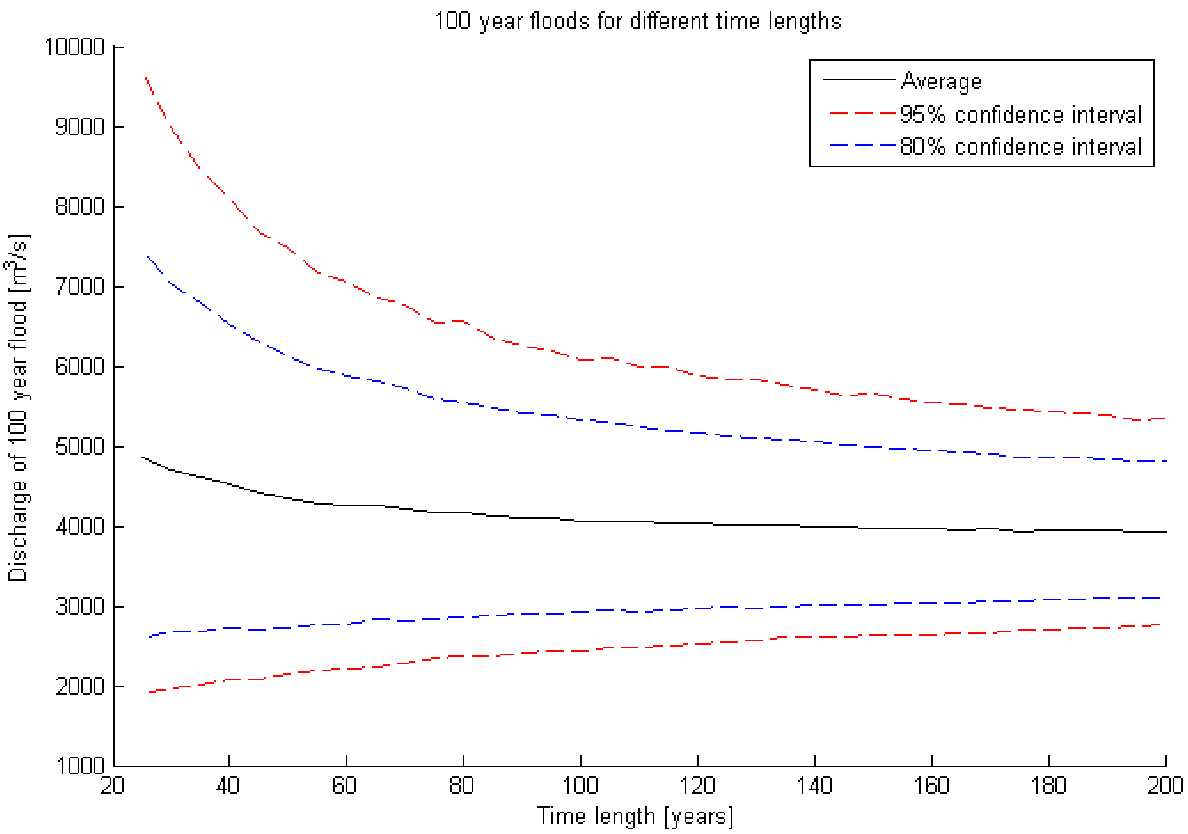

Figure 5-8: Uncertainty in 100 year flood event under ENSO climate variability

As can be seen the confidence intervals are particularly wide at short time lengths. At a data length of only 30 years there is a 5% chance of the true value being either below 2.0 $*10^3$ or above 8.9 $*10^3$ m^3/s. An increased data length does decrease the bandwidth of the confidence limits as can be expected. But even at a data length of 200 years the remaining uncertainty remains large, having a 5% chance of the true value being below 2.7 $*10^3$ or above 5.3 $*10^3$ m^3/s.

5.3 Flood inundation model

A HEC-RAS model is built to estimate the flood inundation area under the different climate states. The general method is explained in Chapter 4.4. The model calibration is described in Appendix I: *HEC-RAS model calibration*. It must be stated that uncertainty exists due to the variety of available rating curves (discharge – height relation) as also explained in Appendix I. Conclusions drawn from this analysis are prone to this uncertainty.

Figure 5-9 (*El Niño and La Niña inundations at upstream boundary cross-section*), Figure 5-10 (*Flood inundation map 100 year La Niña and El Niño flood*) and Table 5-6 *(Flood inundation areas for all conditional 100 year flood events and inundation depths for channel at upstream boundary cross-section)* present the main results gained from the steady flow analysis using the calibrated HEC-RAS model. Cross-section plots and 3-D plots for other events can be found in Appendix J: *Plots of flood inundation model outcomes.*

Table 5-6: 1% AEP flood inundation extent

100 year Flood event	Discharge [m^3/s]	Area of inundation [$*10^3$ m^2]	Water depth [m]
Unconditional	3459.3	849	11.9
El Niño	3439.5	849	11.9
La Niña	5179.2	940	13.9
PDO positive	3010.6	824	11.2
PDO negative	5008.9	940	13.7
Long term flood risk lower 95% confidence limit	2700	776	10.7
Long term flood risk upper 5300 940 **95% confidence limit**	14.0		

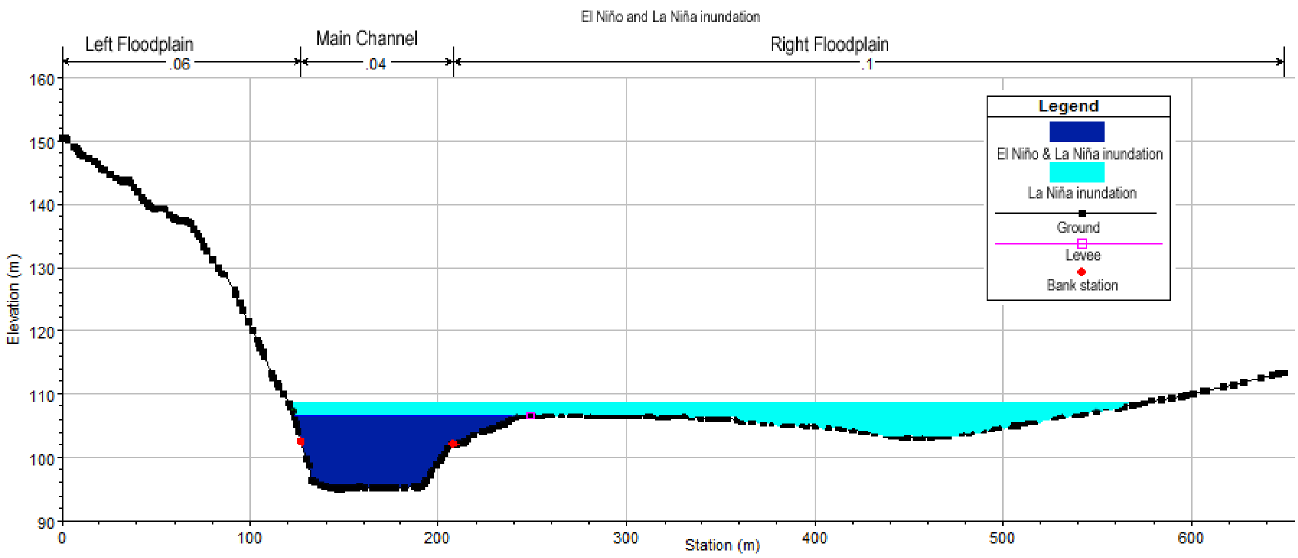

Figure 5-9: El Niño and La Niña inundations at upstream boundary cross-section

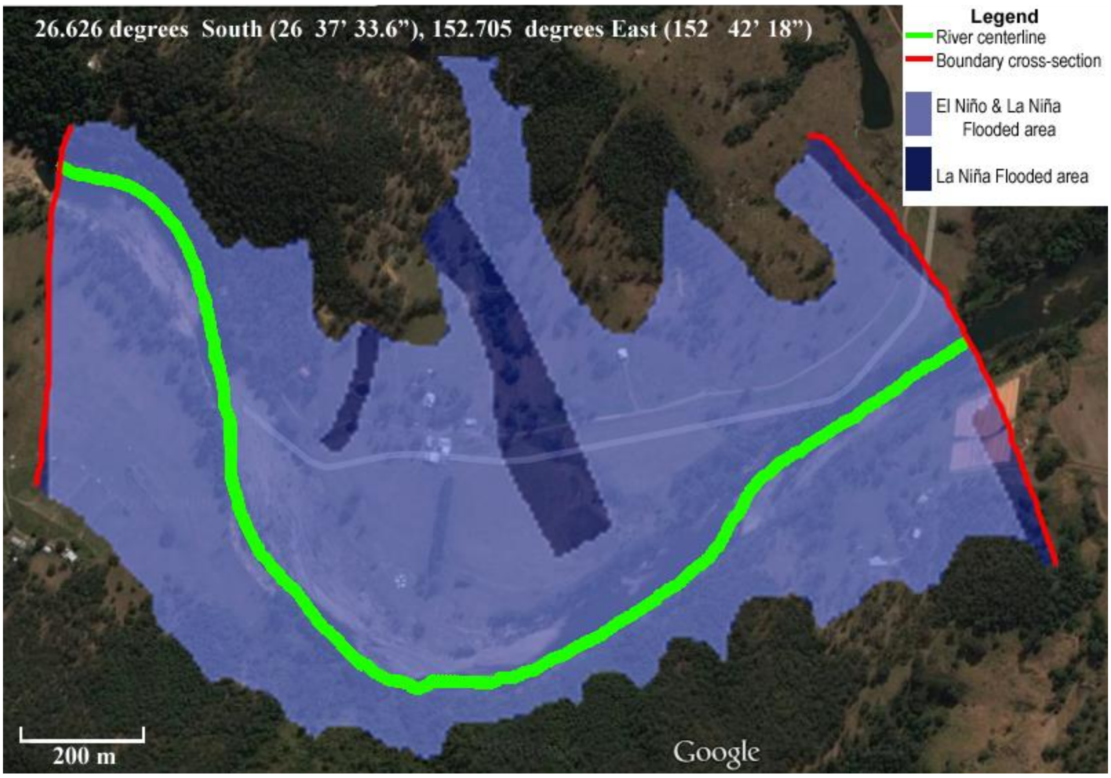

Figure 5-10: Flood inundation map 100 year La Niña and El Niño flood

As becomes evident from Table 5-6 and Figure 5-10 the flood inundation area does not show a high variance under the different climate scenarios (variability modes). The main reason is the terrain of the study area. Both floodplains are delimited by high elevation areas which are preceded by steep slopes (see Figure 3-4 in Chapter 3 for elevation map), whereby the area does not increase significantly once the inundation has exceeded the main channel. However the inundation depths do reflect the effects of increased discharge under different climate scenarios. For the El Niño and La Niña events the difference in flood inundation depth is 2.0 meter as can be seen in the cross-section plot in Figure 5-9. Considering the El Niño and La Niña flood areas both exceed the main channel, the floodplains are also greatly affected.

5.4 Spatial variance of climate variability effects on flood frequencies

The spatial variance in conditional flood frequencies is tested using flow data from several catchment areas in the Eastern Australia. The New South Wales Government's website WaterInfo provides flow data for nearly every catchment area in New South Wales. A variety of data series from different catchment area types are tested. Table 5-7 gives the characteristics of the tested catchment areas for which the locations can be seen in Figure 5-11.

Table 5-7: Catchment characteristics

River name	Gauge	Catchment area [km²]	Data range
Clarence River	Nymboida	1660	1909-2012
Macintyre River	Mungindi	44070	1891-2013
Richmond River	Casino	1790	1943-2013
Namoi River	Gunnedah	17100	1891-2013
Bellinger River	Thora	433	1955-2013

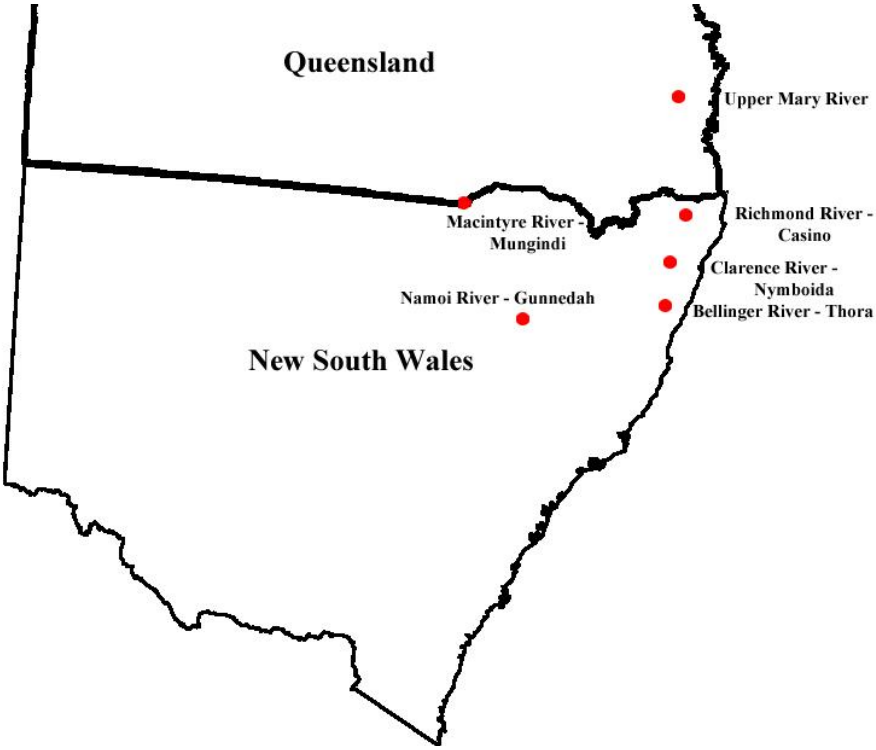

Figure 5-11: Map gauges New South Wales

Table 5-8 and Table 5-9 present the results for the catchment areas in New South Wales for 100 year flood events. The climate variability signals are identified by using the climate variability strength (see 4.1.3).

Table 5-8: New South Wales climate variability strengths for 100 year floods

Catchment Area	Unconditional 100 year flood	IPO strength	PDO strength	ENSO strength
Upper Mary River	3459 m^3/s	0.66	1.66	1.51
Clarence River	5809 m^3/s	2.55	2.08	1.74
Bellinger River	1845 m^3/s	1.38	1.20	1.91
Richmond River	2293 m^3/s	1.46	1.34	1.11
Namoi River	5781 m^3/s	3.29	4.12	3.44
Macintyre River	1171 m^3/s	2.47	2.08	1.21

Table 5-9: New South Wales combined climate variability strengths for 100 year floods

Catchment Area	Combination IPO/ENSO strength	Combination PDO/ENSO strength
Upper Mary River	0.93	1.11
Clarence River	4.36	4.47
Bellinger River	1.67	Insufficient data
Richmond River	0.92	0.86
Namoi River	6.85	8.40
Macintyre River	2.61	2.11

Apparent from Table 5-8 and Table 5-9 is a high spatial variance in climate variability strengths. The Clarence River, Bellinger River and Richmond River for example are all coastal catchment areas in north eastern New South Wales, but still have a certain degree of variance amongst them. Furthermore, using the values in the tables it can be concluded that the PDO and the IPO have a reasonable similarity in strengths amongst the New South Wales catchment; catchments with a weak IPO signal also show a weak PDO signal and reversed. Both in terms of the single climate variability modes as the combination between IPO/PDO and ENSO, the catchments wield very comparable strengths. This contradicts to the Upper Mary River catchment in which the IPO and the PDO did not agree in values.

For the Clarence River Catchment area, the results are presented and discussed in more detail in Appendix K: *Data analysis for Clarence River Catchment*. The most important findings for this catchment area are:

- A strong IPO signal is identified as the 95% confidence bounds of the flood frequency curves of the positive and the negative IPO phases barely overlap showing a significant difference between the flood frequencies in the two phases. Further proof of the strong signal is a very low p-value (0.000).
- The effects of the PDO and the IPO show a high degree of coherence as the flood frequency curves of the two climate variability modes are rather similar. This coherence is expected (2.2), but contradicts to the outcomes of the Upper Mary River as this catchment had a weak IPO signal and a strong PDO signal.
- The long-term uncertainty due to IPO variability is shown to be very large as the 95% confidence bounds are +50% and -50% of the average 100 year flood event.

5.5 Influence climate change

The following future climate scenarios for the climate change effects by 2050 (see 4.5 for descriptions) are assessed in the context of the flood frequency analyses (Chapter 5.1):

1. The return time of the 100 year flood event magnitude is reduced to 30-40 years (Milly, Wetherald , Dunne, & Delworth, 2002)
2. A 10 per cent increase of the 100 year flood event (State of Queensland, 2010)
3. The return time of the 40 year flood event magnitude is reduced to 18 years (Walsh, et al., 2001)

The flood frequencies are based on the deviation from the unconditional flood frequency curves. For scenario 1 and 3 the unconditional flood frequency curve is multiplied by the factor corresponding to the change in return times. Figure 5-12 shows the flood frequencies for these climate scenarios along with the unconditional flood frequency curve and its confidence intervals (5.1.2) and the conditional La Niña flood frequency curve (5.1.3.3).

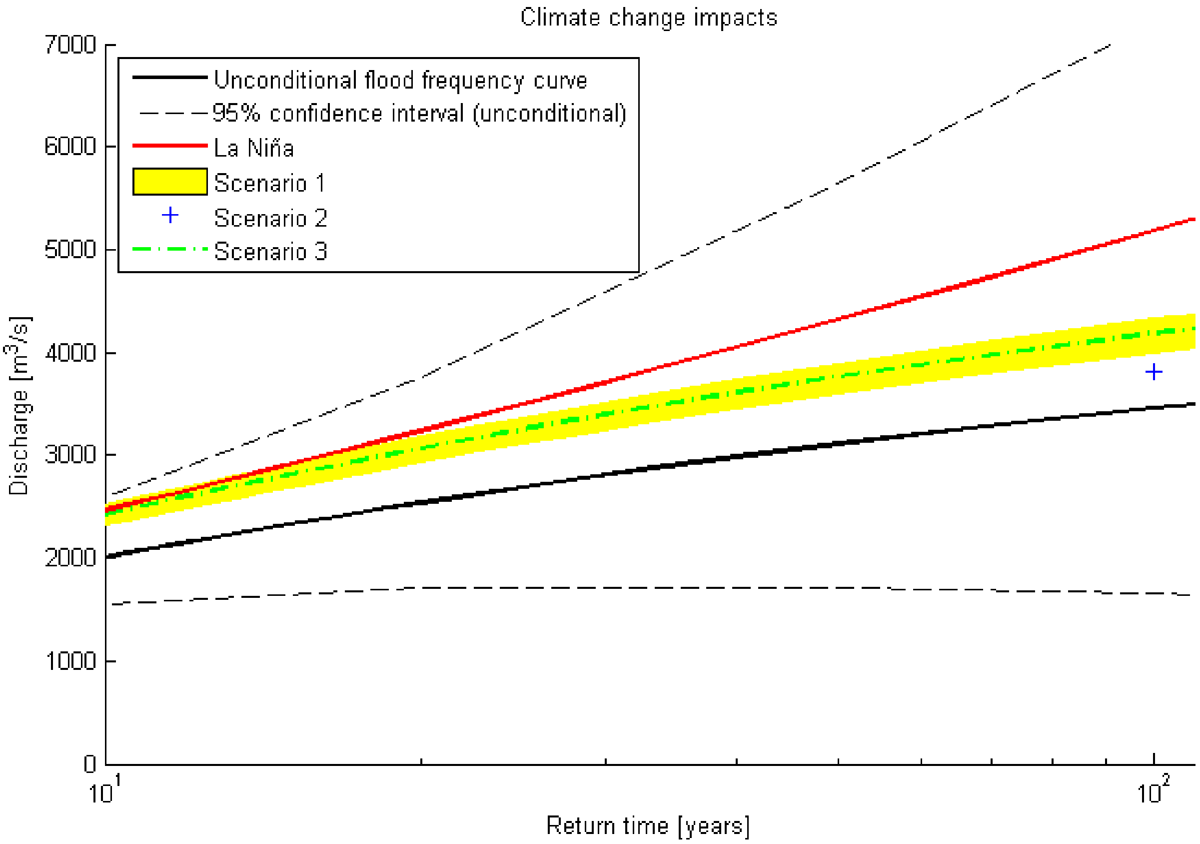

Figure 5-12: Climate change impacts

Judging Figure 5-12 it becomes evident that the climate change effects seem limited in this catchment area. The three scenarios, which are not necessarily representative as it is a selection from a variety of researches which all have different (non-quantitate) predictions, all remain within the 95% confidence bounds of the unconditional model fit, meaning that no significant change (5% significance level) can be proven. Furthermore the flood frequencies under climate change do not exceed the conditional flood frequencies of La Niña events. This would mean that during coming La Niña events the flood risk is higher than in non-La Niña years around 2050. It must be stated though that the uncertainty remains very large, especially because only three quantitative scenarios could be derived (see 2.3 and 4.5). At last it must be stated that using only these results it cannot be proven that climate change does not have a large influence on the flood risks. As this catchment is fairly small the effects are always less evident compared to larger catchments. Therefore to be able to draw a more certain conclusion a larger catchment must also be researched.

6 Discussion and conclusions

In addition to numerous previous studies, this study has again shown the existence and the effect of climate variability, both decadal and multi-decadal.

Firstly an unconditional flood frequency analysis was performed to set the reference situation for further flood analyses. This unconditional flood frequency analysis showed why the Log-Pearson type 3 distribution was the preferred model distribution for this research. Being the best fitting model on visual inspection and model fit parameters, it was chosen to be the leading model distribution throughout the rest of the research. This decision was supported by other data sets also having a good (graphical) fit, judging the results in Chapter 5.1 and Appendix I. Throughout the research the Log-Pearson type 3 distribution was also a steady performing model distribution. However the sensibility to both low and high outliers can become troublesome. An example of this is the model fit for the conditional IPO states. Nearly all values for the ranked negative IPO discharges are higher than the corresponding ranked positive IPO discharges, but due to two high outliers and an increasing trend in low discharge values in the positive series the positive IPO phase ends up with a higher 100 year flood event. This limitation must be kept in mind in for any conclusions drawn from this research. Furthermore it must be said that the uncertainty bounds of the model fits become particularly wide for high return times if there is a limited number of data points (applies to all conditional flood frequency analyses).

As stated just before the conditional IPO model fits did not seem to represent the true situation in the Upper Mary River catchment. The raw observed data (to be seen in 5.1.3.1 and Appendix F) suggest, as expected (2.2) the negative phase having a slightly higher flood frequency. The weak IPO signal for the south east Queensland Upper Mary River catchment is still remarkable since it lies in an area with catchments having the strongest IPO signals of the eastern Australian coast (Micevski, Franks, & Kuczera, 2006).

The analyses of the catchments in New South Wales (in 5.4) shed a light on the differences in climate variability signals. Whereas the Upper Mary River catchment had a very weak IPO signal some of the NSW catchments had a very strong signal. This shows the high spatial variance of the IPO as was also concluded in previous researches (Kuczera & Franks, 2002) (Micevski, Franks, & Kuczera, 2006). Therefore for any flood analysis in Eastern Australia the presence IPO signal must be determined. This is particularly important for any catchment with a limited discharge data length, because the uncertainty for short length data sets is shown to be very large if the catchment is affected by climate variability (see 5.2 and 5.4). But also if a 200-year data set is available the uncertainty remains large. In the Upper Mary River this uncertainty was expressed in a water level difference of 2.0 meters. For more populated areas in Queensland and New South Wales uncertainties in flood risk estimation are potentially catastrophic as flood risks can be drastically underestimated. For future flood risk analyses this uncertainty should therefore be assessed as the analyses can be in great error.

On top of the uncertainty of current climate variability is the uncertainty due to future climate changes. For Eastern Australia the effects of climate change on flood risks are unclear (2.3). Whereas past trends of 1970 onwards showed a decreasing frequency and magnitude of extreme events, many researchers predict higher flood risks across Eastern Australia. Due to the low number of quantitative predictions the possible changes to the mean state of the climate could only be partially evaluated for the Upper Mary River catchment. The few scenarios that were evaluated did not show significant changes to the average flood frequencies. To assess if climate change will have an effect on the average flood frequencies further research is required, whereby more recent climate change scenarios should be applied.

In the light of the high uncertainty in flood frequency analyses due to climate variability, future researches need to assess the contribution of climate change to this uncertainty. As the El Niño Southern Oscillation has a major effect on the flood risk in Eastern Australia possible future changes in the frequency and magnitude of El Niño and La Niña events have a strong effect on the flood risks. The changes in global climate can potentially alter the climate mechanisms which cause climate oscillations. The effect of climate change on the frequency and magnitude of climate variability modes is an ongoing topic of research and the outcomes of these researches are of great importance to predict future flood risks.

7 References

Arcement Jr., G., & Schneider, V. (1984). *Guide for Selecting Manning's Roughness Coefficients for Natural Channels and Flood Plains.* United States Geological Survey Water .

Australia's BOM Climate Analysis Section. (2014, July). *S.O.I. (Southern Oscillation Index) Archives.* Retrieved July 14, 2014, from Bureau of Meteorology Climate: http://www.bom.gov.au/climate/current/soihtm1.shtml

Biondi, D., Freni, G., Iacobellis, V., Mascaro, G., & Montanari, A. (2012). Validation of hydrological models: Conceptual basis, methodological approaches and a proposal for a code of practice. *Physics and Chemistry of the Earth, 42-44*, 70-76.

Brunner, & Gee. (2005). *Boundary and Initial Conditions.* National Oceanic and Atmospheric Administration, Service, U.S. National Weather.

Bureau of Meteorology; Australian Government. (2014). *Australian rainfall patterns during La Niña events*. (Australian Government) Retrieved January 4, 2014, from ENSO-Wrap up: http://www.bom.gov.au/climate/enso/ninacomp.shtml

Bureau of Meteorology; Australian Government. (2014). *Southern Oscillation Index*. (A. Government, Producer) Retrieved January 4, 2014, from Bureau of Meteorology Climate Glossary: http://www.bom.gov.au/climate/glossary/soi.shtml

Bureau of Meteorology; Australian Government. (n.d.). *Australian Climate Extremes - Trend Maps*. Retrieved July 24, 2014, from BOM Climate Change: http://www.bom.gov.au/climate/change/index.shtml#tabs=Tracker&tracker=extremes-trend-maps

Climate Analysis Section. (2008, May). *TNI (Trans-Niño Index) and N3.4 (Niño 3.4 Index).* Retrieved July 11, 2014, from Climate and Global Dynamics Division - Climate Analysis Section: http://www.cgd.ucar.edu/cas/catalog/climind/TNI_N34/index.html

Collins, M. (2005). El Niño- or La Niña-like climate change? (The CMIP Modelling Groups, Red.) *Climate Dynamics, 24*, 89 - 104.

Collins, M., An, S.-I., Cai, W., Ganachaud, A., Guilyardi, E., Jin, F.-F., et al. (2010, June). The impact of global warming on the tropical Pacific Ocean and El Niño. *Nature Geoscience, 3*, 391 - 397.

CSIRO. (2001). *Australia State of the Environment Report 2001.* Bureau of Meteorology; Australian Government.

CSIRO. (2014). *State of the Climate 2014*. Retrieved July 31, 2014, from CSIRO climate change: http://www.csiro.au/Outcomes/Climate/Understanding/State-of-the-Climate-2014/Heavy-Rainfall-and-Tropical-Cyclones.aspx

CSIRO and Bureau of Meteorology. (2014). *State of the climate 2014.* Australian Government.

Department of the Environment; Australian Government. (n.d.). *Sea Level*. Opgeroepen op July 24, 2014, van Climate change in the future: http://www.climatechange.gov.au/climate-change/climate-science/climate-change-future/sea-level

Djokic, D., & Maidment, D. R. (2012, April 9). Introduction to HEC-RAS and Floodplain Mapping. Austin: University of Texas.

Easdown, G. (2011, January 15). Counting cost of Queensland floods. *news.com.au*.

Erik K. Veland. (2011, January). *La Niña Related Impacts Likely to Continue.* (I.-C. University, Ed.) Retrieved January 4, 2014, from IRI publications: http://iri.columbia.edu/docs/features/2011_spotlight_features/la_nina_related_impacts_likely_to_continue.html

Federal Emergency Management Agency. (2002). *HEC-RAS procedures for HEC-2 Modelers.* Washington DC.

Franks, S. (2014). Chapter 23: Flood Risk in Eastern Australia - Climate Variability and Change. In K. Beven, & J. Hall, *Applied Uncertainty Analysis for Flood Risk Management* (pp. 605 - 624). Imperial College Press.

Franks, S. (n.d.). Peak Flow Estimation. University of Tasmania.

Google. (2014). Retrieved July 23, 2014, from Google Maps: https://www.google.com.au/maps/@-26.6232434,152.705989,15z

Hadley Centre Sea Ice and Sea Surface Temperature. (2014, April). *Niño 3.4 long data.* Retrieved July 11, 2014, from Earth Sciences Research Laboratory - Physical Sciences Division: http://www.esrl.noaa.gov/psd/gcos_wgsp/Timeseries/Data/nino34.long.data

Hughes, L. (2003). Climate change and Australia: Trends, projections and impacts. *Austral Ecology, 28*, 423 - 443.

Hydraulic Engineering Center. (n.d.). *HEC-GeoRAS*. (U.S. Army Corps of Engineers) Retrieved June 16, 2014, from Hydraulic Engineering Center Software: http://www.hec.usace.army.mil/software/hec-georas/

IPCC, W. G. (2007). *Chapter 3.6.3: Pacific Decadal Variability*. Opgeroepen op August 7, 2014, van IPCC Fourth Assessment Report: Climate Change 2007; The Physical Science Basis: http://www.ipcc.ch/publications_and_data/ar4/wg1/en/ch3s3-6-3.html

Kiem, A. S., & Franks, S. W. (2001). On the identification of ENSO-induced rainfall and runoff variability: a comparison of methods and indices. *Hydrological Sciences Journal, 46*(5), 715-727.

Kiem, A. S., Franks, S. W., & Kuczera, G. (2003). Multi-decadal variability of flood risk. *Geophysical Research Letters, 30*(2), 1035-1038.

Kuczera, G., & Franks, S. W. (2002). Flood frequency analysis: Evidence and implications of secular climate variability, New South Wales. *Water Resources Research, 38*(5), 1062.

Mann, M., Bradley, R., & Hughes, M. (2000, November). *Global Temperature Patterns in Past Centuries: An Interactive Presentation*. Retrieved July 29, 2014, from World Data Center for Paleoclimatology and NOAA Paleoclimatology Program: https://www.ncdc.noaa.gov/paleo/ei/ei_data/ninoann-recon.dat

Mantua, N. (2002). Pacific–Decadal Oscillation (PDO). (M. MacCracken, & J. Perry, Red.) *Encyclopedia of Global Environmental Change, 1; The Earth system: physical and chemical dimensions of global environmental change*, 592-594.

Mantua, N. (2014, June). *PDO index.* Opgeroepen op July 22, 2014, van Joint Institute for the Study of Atmosphere and Ocean - College of the Environment - University of Washington: http://jisao.washington.edu/pdo/PDO.latest

Meehl, G., & Washington, W. (1996, July 4). El Niño-like climate change in a model with increased CO2 concentrations. *Letters to nature, 382*, 56-60.

Merwade, V. (2012, June). *Tutorial on using HEC-GeoRAS with ArcGIS 10 and HEC-RAS Modeling.* Purdue University, Schoon of Civil Engineering.

Micevski, T., Franks, S. W., & Kuczera, G. (2006). Multidecadal variability in coastal eastern Australian flood data. *Journal of Hydrology, 327*, 219 - 225.

Milly, P., Wetherald , R., Dunne, K., & Delworth, T. (2002, January 31). Increasing risk of great floods in a changing climate. *Letters to Nature, 415*, 514 - 517.

Ministry for the Environment New Zealand. (n.d.). *23 Factsheet 12: ENSO and IPO.* Retrieved June 12, 2014, from Climate change publications: https://www.mfe.govt.nz/publications/climate/coastal-hazards-climate-change-guidance-manual/page24.html

Murphy, B., & Timbal, B. (2008). A review of recent climate variability and climate change in southeastern Australia. *International Journal of Climatology, 28*, 859 - 879.

National Climatic Data Center. (n.d.). *PDO teleconnection*. (National Oceanic and Atmospheric Administration - US Government) Retrieved July 10, 2014, from National Climatic Data Center website: http://www.ncdc.noaa.gov/teleconnections/pdo.php

NOAA Fishery Service. (2011, January). Retrieved June 16, 2014, from http://www.habitat.noaa.gov/pdf/flood_frequency_estimates.pdf

Parker, D., Folland, C., Scaife, A., Knight, J., Colman, A., Baines, P., et al. (2007). Decadal to multidecadal variability and the climate change background. *Journal of Geophysical Research, 112*, D18115.

Philip, S. Y. (2009). *Exploring El Niño mechanisms in climate models.* Royal Netherlands Meteorological Institute.

Power, S., Casey, T., Folland, C., Colman, A., & Mehta, V. (1999). Inter-decadal modulation of the impact of ENSO on Australia. *Climate Dynamics, 15*, 319-224.

Royal Dutch Meteorological Insitute. (n.d.). *Effects of El Niño on global weather*. Retrieved January 4, 2014, from Weather expactations: http://www.knmi.nl/waarschuwingen_en_verwachtingen/seizoensverwachting/effecten/

Salinger, M., Renwick, J., & Mullan, A. (2001, May 8). Interdecadal Pacific Oscillation and South Pacific climate. *International Journal of Climatology, 21*, 1705-1721.

Smythe, C. (2014, June 20). Upper Mary River catchment data. Queensland, Australia: Sunshine Coast Regional Council.

State of Queensland. (2010). *Increasing Queensland's resilience to inland flooding in a changing climate: Final report on the Inland Flooding Study.* Department of Environment and Resource Management, Department of Infrastructure and Planning and Local Government Association of Queensland.

Timmermann, A., Oberhuber, J., Bacher, A., Esch, M., Latif , M., & Roeckner, E. (1999, April 22). Increased El Niño frequency in a climate model forced by future greenhouse warming. *Letters to Nature, 398*, 694 - 697.

Trenberth, K., & Hoar, T. (1997, December 1). El Niño and Climate Change. *Geophysical Research Letters, 24*(23), 3057-3060.

U.S. National Climatic Data Center. (2011, May). *Interdecadal modulation of El Niño amplitude during the past millennium.* Retrieved July 15, 2014, from NOAA paleoclimatology: http://www.ncdc.noaa.gov/paleo/pubs/li2011/li2011.html

U.S. Water Advisory Committee on Water Data. (1982). *Guidelines for determining Flood Flow Frequency - Bulletin 17B of the Hydrology Subcommittee.* U.S. Department of the Interior Geological Survey.

Van den Honert, R. C., & McAneney, J. (2011). The 2011 Brisbane Floods: Causes, Impacts and Implications. *Water, Vol. 3*, 1149-1173.

Verdon, D. C., & Franks, S. W. (2006). Long-term behaviour of ENSO: Interactions with the PDO over the past 400 years inferred from paleoclimate records. *Geophysical Research Letters, 33*(L06712).

Walsh, K., Hennessy, K., Jones , R., McInnes, K., Page, C., Pittock, B., et al. (2001). *Climate Change in Queensland under Enhanced Greenhouse Conditions* . CSIRO.

Wenju, C., & Van Rensch, P. (2012, April 25). The 2011 southeast Queensland extreme summer rainfall: A confirmation of a negative Pacific Decadal Oscillation phase? *39*(8).

Whetton, P., Fowler, A., Haylock, M., & Pittock, A. (1993). Implications of climate change due to the enhanced greenhouse effect on floods and drought in Australia. *Climatic Change, 25*, 289-317.

Wolter, K. (2011, May 10). *MEI values.* Retrieved July 11, 2014, from Earth System Research Laboratory - Physical Sciences Division: http://www.esrl.noaa.gov/psd/enso/mei.ext/table.ext.html

Wolter, K., & Timlin, M. (1998). Measuring the strength of ENSO—how does 1997/98 rank? *Weather, 53*, 315-324.

Yuan, Y., & Qaiser, K. (2011). *Floodplain Modeling in the Kansas River Basin Using Hydrologic Engineering Center (HEC) Models.* United States Environmental Protection Agency, Research and development.

Zhang, X., & Church, J. A. (2012, November 1). Sea level trends, interannual and decadal variability in the Pacific Ocean. *Geophysical research letters*, L21701.

Appendices

Appendix A. Discharge data extension Bellbird Creek using Kenilworth gauge data

As mentioned in the main document the data series of the Bellbird Creek can be extended back to 1926. To extend the discharge data set of the Bellbird creek the data of the Kenilworth gauge is used. The two gauges have operated concurrently from 1959 until 1973. The peaks of 1961 are not included as there was no continuous discharge data set available for this year at the Kenilworth gauge. The yearly discharge peaks that have occurred at the two gauges in this period are given in Table A-1. These peaks have been derived under the assumption of a hydrological year from October-September.

Table A-1: Peak (log-) discharges Bellbird Creek and Kenilworth

Year	Peak discharge Bellbird Creek [m³/s]	Peak discharge Kenilworth [m³/s]
1959	1211.6	1162.7
1960	86.7	101.4
1961	97.2	No data
1962	72.3	144.8
1963	1889.4	1343.1
1964	417.7	821.1
1965	504.9	692.8
1966	119.0	23.4
1967	1081.5	1089.8
1968	2142.7	1563.2
1969	40.7	64.5
1970	222.1	566.5
1971	1262.4	1078.3
1972	1624.8	1672.1
1973	1817.9	1546.7

The discharge peaks and the fitted log-log relationship (bases 10) are shown in Figure A-1.

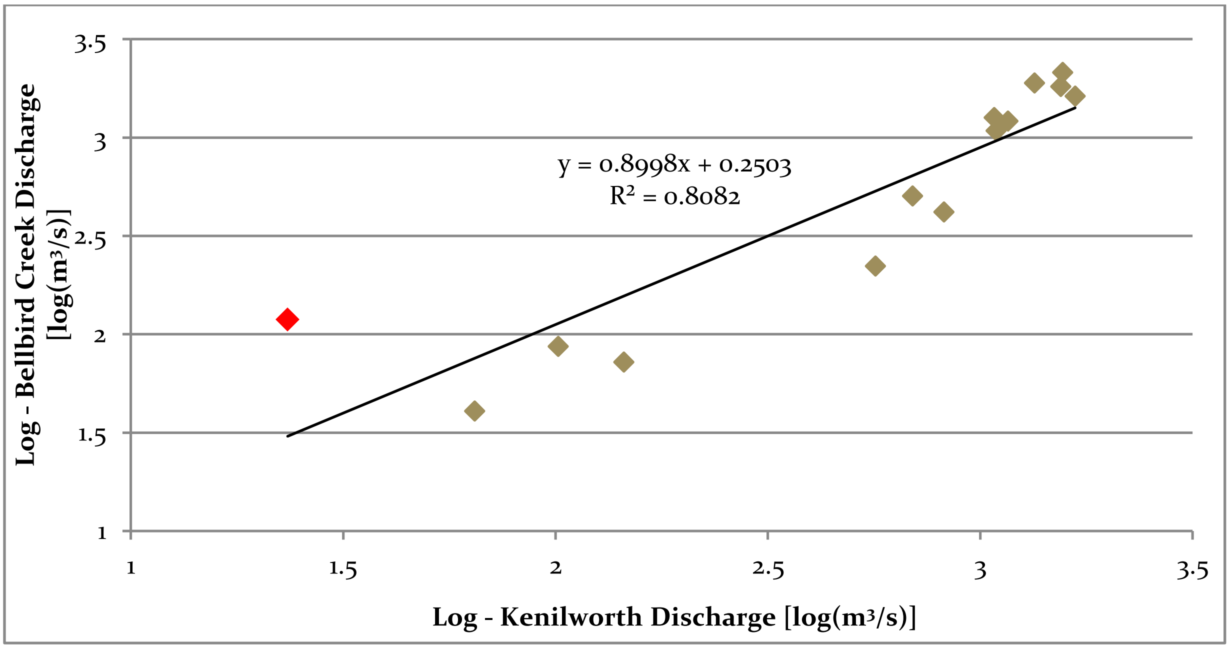

Figure A-1: Log-Log relationship for Bellbird Creek and Kenilworth including outlier

As becomes evident from the plot and the tabulated values one outlier exists, 1966's peaks do not match. The outlier has been marked red in the plot and the table. As the gauge in Kenilworth is downstream of the gauge in the Bellbird Creek and after the confluence of the Bellbird Creek with the Obi Obi Creek (see Figure 3-1), it is highly unlikely the discharge can be significantly lower at Kenilworth. Reasons for the observed differences can be:

- Extraction of water
- High deviations in the rating curve for very low discharges (23.4 m^3/s at Kenilworth)
- Absence of a continuous measurement at the time of the Bellbird Creek peak in 1966

For the reasons of unlikelihood and the 1966 peak being an extreme dry event for the Kenilworth gauge, 1966 is considered as an outlying event and ruled out of the relation. The removal of this data point leads to the relation as displayed in Figure A-2. The Coefficient of correlation (R^2) is improved, having a value of 0.808 before the removal which increases to 0.938 after the removal.

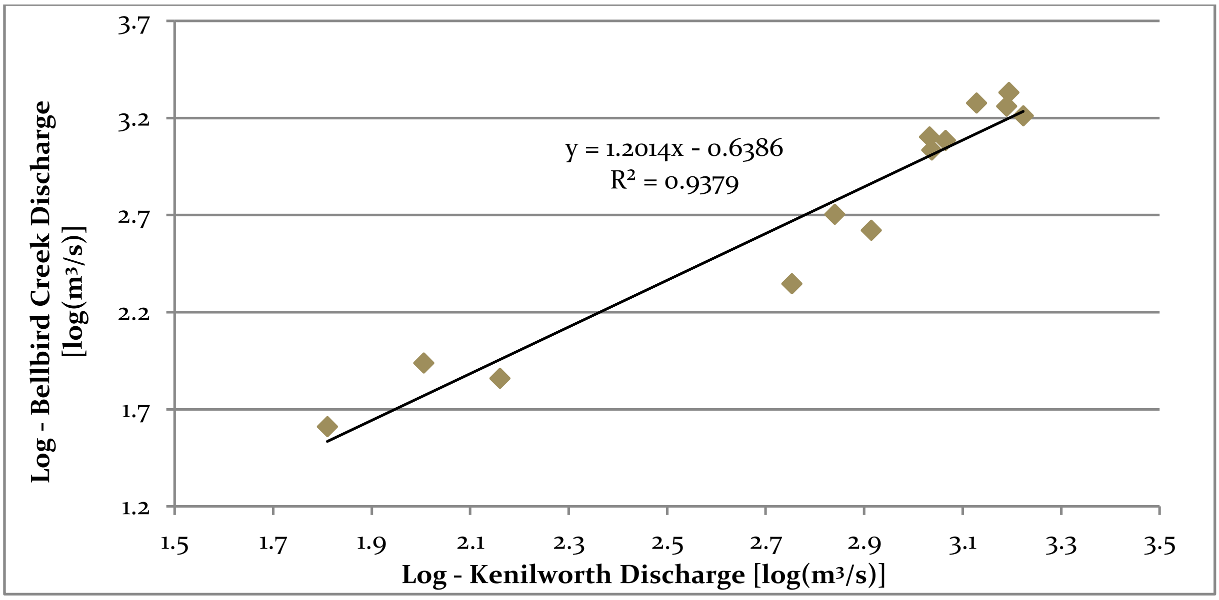

Figure A-2: Log-Relationship Kenilworth-Bellbird Creek

Figure A-2 proves a strong correlation between the discharges in the Bellbird Creek and the Mary River at Kenilworth. This correlation was expected as the gauge in Kenilworth is located directly downstream of the Bellbird Creek gauge (see Figure 3-1). This log-log relationship is used to extend the data series to 1926, the year in which the Kenilworth gauge started operation.

Appendix B. Log-Pearson type 3 fitting

The method described below is based on the Australian Rainfall and Runoff guidelines (Franks S. , n.d.).

The general formula that describes the Log-Pearson 3 distribution is as follows:

$$Q = 10^{\mu + {}^{III}K_p \sigma}$$

Q	=	Model discharge
μ	=	Mean of logarithmic values (base 10) of observed data
σ	=	Standard deviation of logarithmic values of observed data
$^{III}K_P$	=	$\dfrac{2\left\{\left[\frac{\eta}{6}\left(K_P-\frac{\eta}{6}\right)+1\right]^3-1\right\}}{\eta}$

K_P	=	Standard normal deviate with probability P (normal distribution with μ = 0 and σ = 1)
η	=	Skew of logarithmic values of observed data

The values of $^{III}K_P$ are tabulated or can be calculated (continuously) using the given formula when the skew is between -1 and 1. In this research the continuous function is used as long as the skew does not exceed the limits.

To determine the confidence limits the following general formula is used:

$$Confidence\ limit(Q) = 10^{\log(Q) \pm \frac{F * \delta * \sigma}{\sqrt{N}}}$$

Q	=	Model discharge
σ	=	Standard deviation of logarithmic values of observed data
N	=	Number of values in the data series
F	=	Normal Frequency factor for desired confidence limit (1.645 represents 95% confidence limit)
δ	=	Tabulated parameter which determines error for LP3 distributions

Since the value of δ is tabulated for a limited amount of return times the confidence limit is determined for the tabulated values only (13 values, AEP 0.995-0.005). The table includes values for skew values between -1.5 and 1.5 with intervals of 0.1. All other skew values between the limits are to be interpolated.

Appendix C. Flowchart of Matlab-model

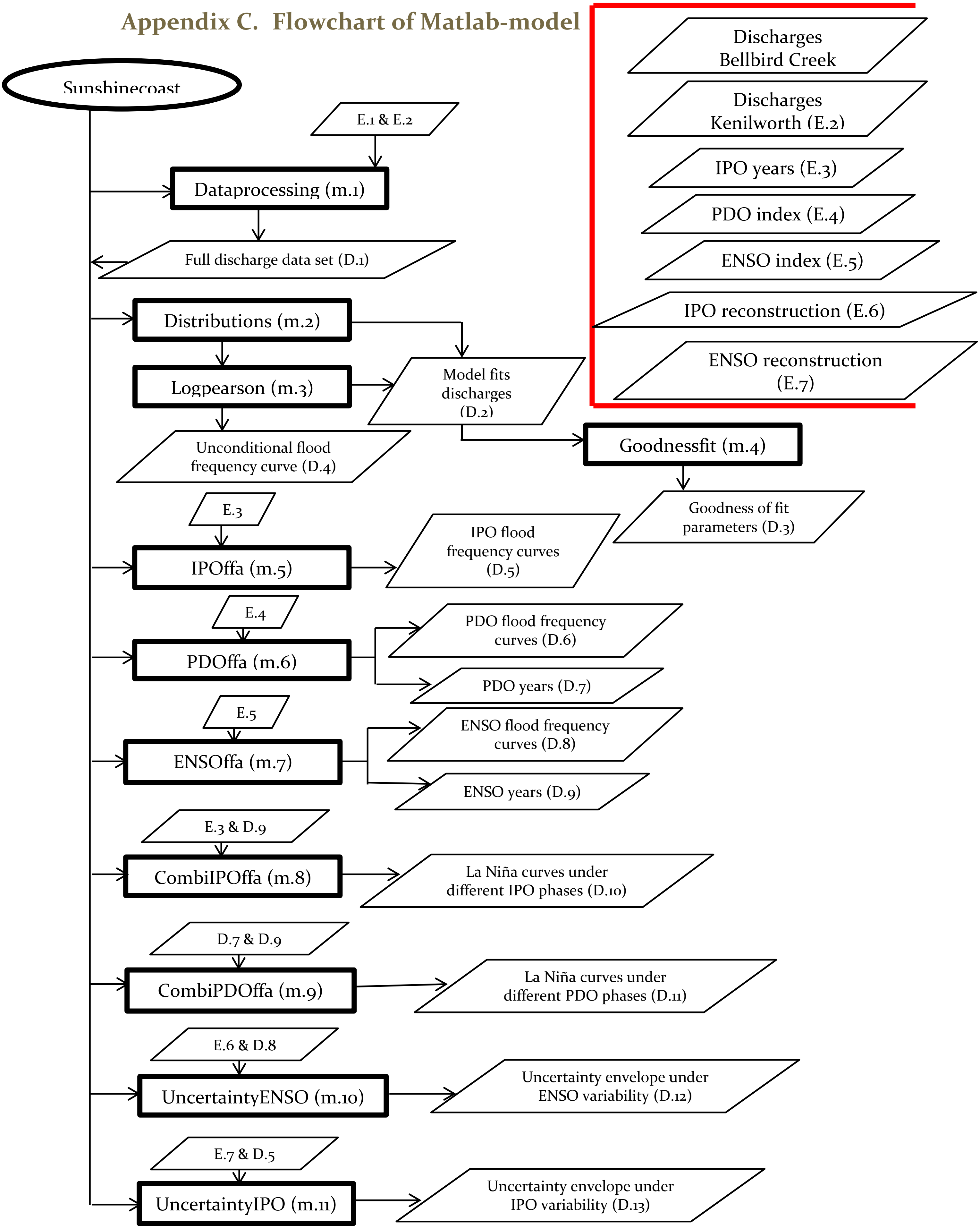

C.1 Model functions

M.1 – Dataprocessing	*Dataprocessing* creates the full discharge data set out of the two separate Kenilworth and Bellbird Creek data set; see Chapter 3 and Appendix A. For other catchment areas this function is logically not used. Figure 3-2 in the main report is the visual outcome of the results of this function.
M.2 – Distributions	*Distributions* fits a set of discharges to four distributions models: Lognormal, Gumbel, GEV and Log-Pearson 3. The output of this function are the fitted discharge data sets (Figure 5-1) and the unconditional flood frequency curve (Figure 5-2). It follows the methodology described in 4.1.1.
M.3 – Logpearsonfit	*Logpearsonfit* is a separate function that fits any discharge data series to a Log Pearson type 3 distribution. It is used for every conditional flood frequency analysis. See Appendix A for the description of how the Log Pearson type 3 fitting is executed.
M.4 – Goodnessfit	*Goodnessfit* calculates and displays the following goodness of fit parameters: Coefficient of Determination (R^2), Root Mean Square Error (RMSE) and Index of Agreement (D). See 5.1.1 for methods and formulas and Table 5-1 for the outcomes of this function for the Upper Mary River catchment area.
M.5 – IPOffa	*IPOffa* performs a flood frequency analysis for the conditional phases of the IPO by calculating and displaying the conditional positive and negative IPO flood frequency curves. It separates the discharges into the defined IPO phases (see 4.2.1) and uses the *Logpearsonfit* function to calculate the curves. The resultant curves for the Upper Mary River can be found in Figure 5-3.
M.6 – PDOffa	*PDOffa* performs a flood frequency analysis for the PDO phases. Firstly it identifies the PDO phases using the input of the PDO index (see 4.2.2 for method). Subsequently it fits the discharges corresponding to the positive and the negative phases using *Logpearsonfit* (see Figure 5-4 for results of Upper Mary River).
M.7 – ENSOffa	*ENSOffa* performs a flood frequency analysis for the ENSO phases. It follows the same steps as *PDOffa* (see 4.2.3 for ENSO identification and Figure 5-5 for results)
M.8 – CombiIPOffa	*CombiIPOffa* first splits the La Niña events' discharges according to the IPO phases, creating two discharge data sets. These discharges are fitted to Log Pearson 3 distributions to create the flood frequency curve for La Niña years in IPO negative phases and the curve for La Niña years in IPO positive phases (results in Figure 5-6).

M.9 – CombiPDOffa

CombiPDOffa follows the same pattern as *CombiIPOffa* but yielding the PDO phases instead of the IPO phases; see Figure 5-7 for results.

M.10 – UncertaintyENSO

UncertaintyENSO executes a Monte-Carlo simulation to calculate the uncertainty of flood estimations as a function of different data lengths. The structure of the function follows the flow chart presented in Figure 4-1. The resultant uncertainty envelopes are found in Figure 5-8.

M.11 – UncertaintyIPO

UncertaintyIPO has the same structure as *UncertaintyENSO,* but logically using the IPO reconstruction instead of the ENSO reconstruction. The uncertainty due to IPO variability was not estimated for the Upper Mary River. However an uncertainty envelope for IPO variability is created for the Clarence River catchment, to be seen in Figure K-9 of 0.

Appendix D. Description of ArcGIS-model

In general the guidelines are followed as suggested by Merwade (2012) and Yuan & Qaiser (2011). Listed below are the steps taken to create the input for HEC-RAS using the ArcGIS-extension HEC-GeoRAS. The ArcGIS-output is shown in Figure D-1.

1. River centreline (Dark blue): the river-centreline is drawn empirically along the deepest points of the river cross-sections.
2. River bank lines (Red): the bank lines mark the switch from the river channel to the river banks or floodplains. These are necessary to have HEC-RAS assign a different manning n roughness coefficient to the river banks. The bank lines are drawn at the point where the slope of the terrain (in the cross-sectional direction) is lower, marking a flatter terrain. The bank points, created at the intersections of the bank lines and the cross-section lines, can be altered in HEC-RAS when necessary.
3. Flow lines (Cyan): the flow lines are used by HEC-RAS to calculate the reach lengths. HEC-RAS requires three flow lines: channel flow line and the bank flow lines. The channel flow line is copied from the river centreline. The bank lines are drawn at an estimated 1/3 of the flood plain width (Merwade, 2012). The downstream reach lengths evaluate the effects of a meandering river.
4. Cross-section lines/XS-Cutlines (Green): the lines marking the cross-sections of the river are drawn empirically perpendicular to the (imaginary) flood direction. The converted three-dimensional XS-cutlines must go up to a sufficient height, since the water level may not exceed the cross-section terrain.
5. Levees (Pink): levee lines are drawn in order to mark a barrier in a cross-section of the river. One limitation of HEC-RAS is the inability to distinguish low-elevation flood plains from the main channel. If the water level would exceed the flood plain elevation, it would consider it flooded, independent of it being connected to the channel or not. A levee is used to avoid areas being considered flooded, when it is geographically impossible. They are positioned at the highest point of the terrain in between the low-elevation part of the flood

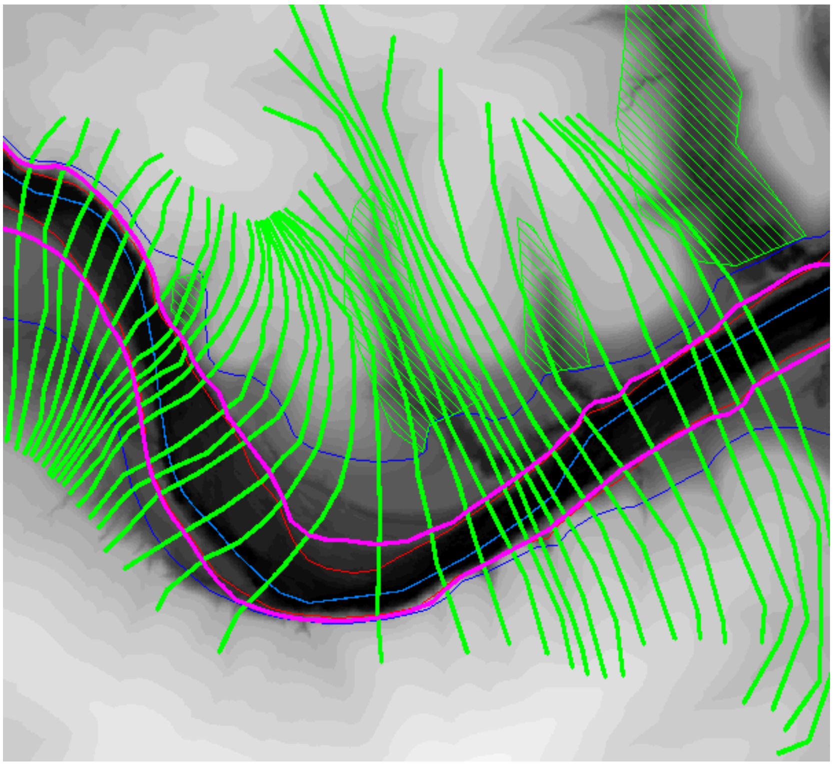

Figure D-1: ArcGIS model output

plain and the main channel. It must be taken into account though that water may be able to flow into the floodplains upstream, a levee for the same secondary channel may thus never exceed the upstream levee height.

6. Ineffective flow areas (Green diagonal lines in an area): Ineffective flow areas are defined as areas in which very little flow is possible. The coves on the left floodplain of the river have been set as and ineffective flow area.

Appendix E. List of years and corresponding climate states

Year	ENSO	PDO	IPO	Year	ENSO	PDO	IPO
1926	o	o	+	1972	+	o	-
1927	o	o	+	1973	-	-	-
1928	o	o	+	1974	-	-	-
1929	+	o	+	1975	-	-	-
1930	+	+	+	1976	+	+	-
1931	o	o	+	1977	+	o	-
1933	-	+	+	1978	o	o	+
1934	o	+	+	1979	+	+	+
1935	o	+	+	1980	o	+	+
1936	o	+	+	1981	o	o	+
1937	o	o	+	1982	+	+	+
1938	-	o	+	1983	o	+	+
1941	+	+	+	1984	-	+	+
1945	o	-	-	1985	o	+	+
1946	o	o	-	1986	+	+	+
1947	o	o	-	1987	+	+	+
1948	o	-	-	1988	-	o	+
1949	-	-	-	1989	o	o	+
1950	-	-	-	1990	o	-	+
1951	+	-	-	1991	+	+	+
1952	o	o	-	1992	+	+	+
1953	o	o	-	1993	+	+	+
1954	-	-	-	1994	+	o	+
1955	-	-	-	1995	o	+	+
1956	-	o	-	1996	o	+	+
1958	+	o	-	1997	+	+	+
1959	o	o	-	1998	-	-	+
1960	o	o	-	1999	-	-	?
1961	-	-	-	2000	-	o	?
1962	o	-	-	2001	o	o	?
1963	+	-	-	2002	+	+	?
1964	-	o	-	2003	o	+	?
1965	+	o	-	2004	+	+	?
1966	o	-	-	2005	o	o	?
1967	-	o	-	2006	+	o	?
1968	+	o	-	2007	-	-	?
1969	+	o	-	2008	-	-	?
1970	-	-	-	2009	+	o	?
1971	-	-	-	2010	-	-	-

Appendix F. Stratified observed discharge data according to identified climate states

Interdecadal Pacific Oscillation positive and negative phases

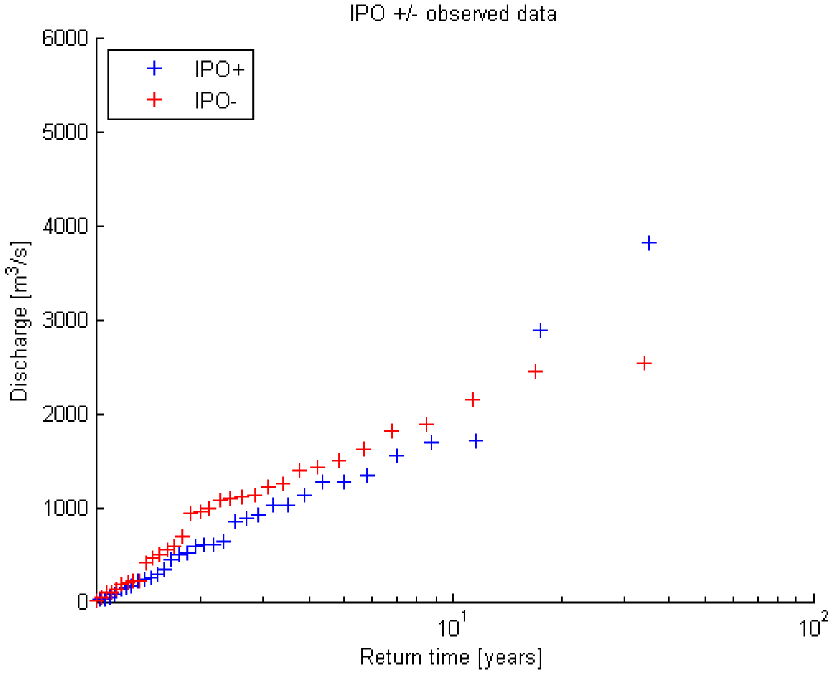

Figure F-1: Observed split data for IPO positive and negative phase(s)

Pacific Decadal Oscillation positive, neutral and negative phases

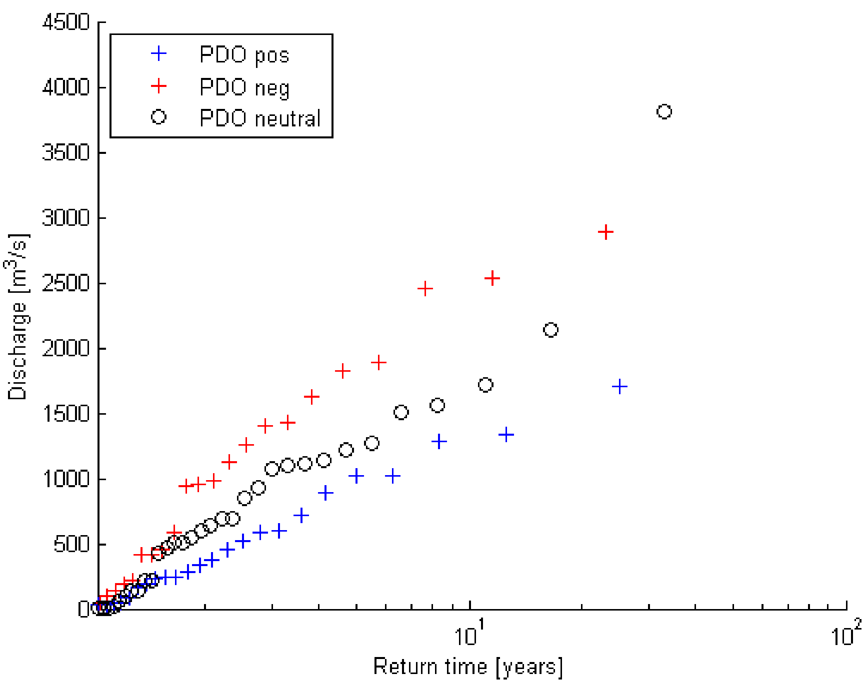

Figure F-2: Observed split data for PDO positive, neutral and negative phase(s)

El Niño Southern Oscillation positive, neutral and negative phases

Southern Oscillation Index (SOI), 6 month average:

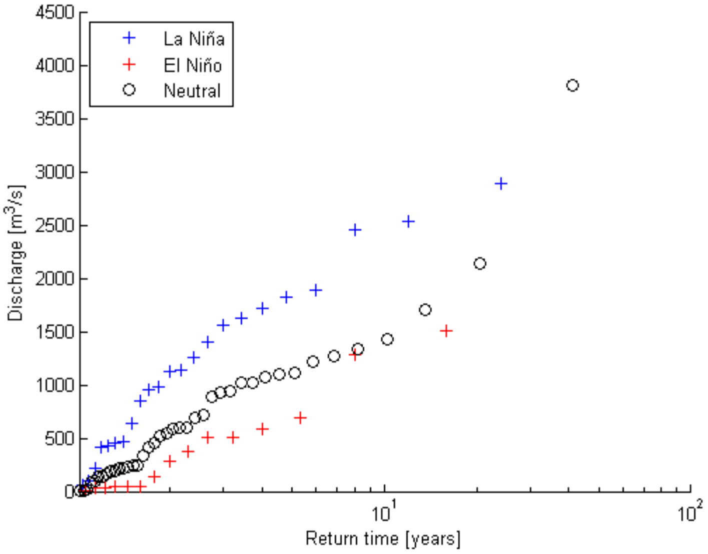

Figure F-3: Observed split data for ENSO positive, neutral and negative phase(s) using the SOI

NINO 3.4 index, 6 month average:

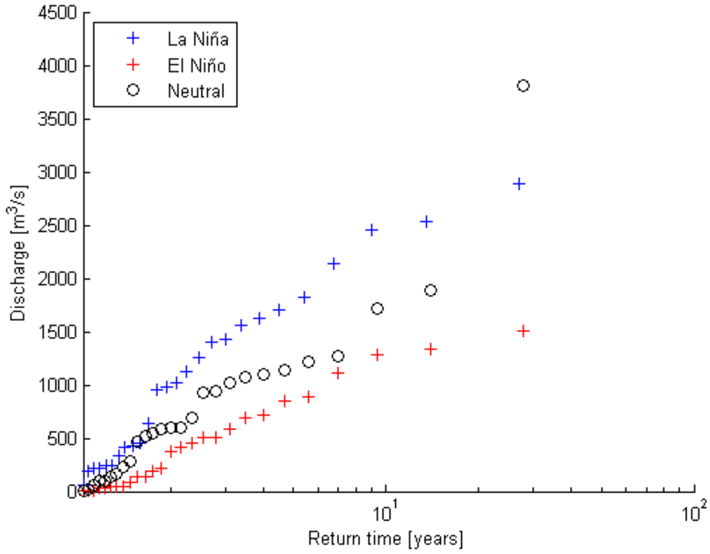

Figure F-4: Observed split data for ENSO positive, neutral and negative phase(s) using the NINO 3.4 index

Multivariate ENSO Index (MEI), 6 month average:

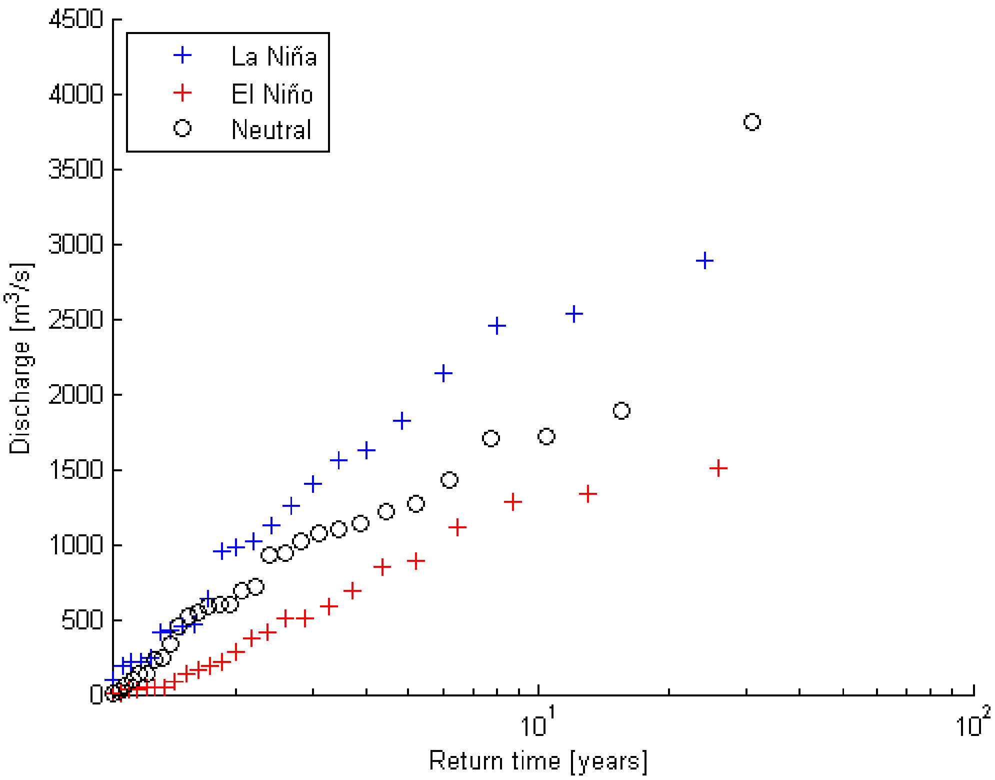

Figure F-5: Observed split data for ENSO positive, neutral and negative phase(s) using the MEI

El Niño years in positive IPO years and La Niña years in negative IPO years

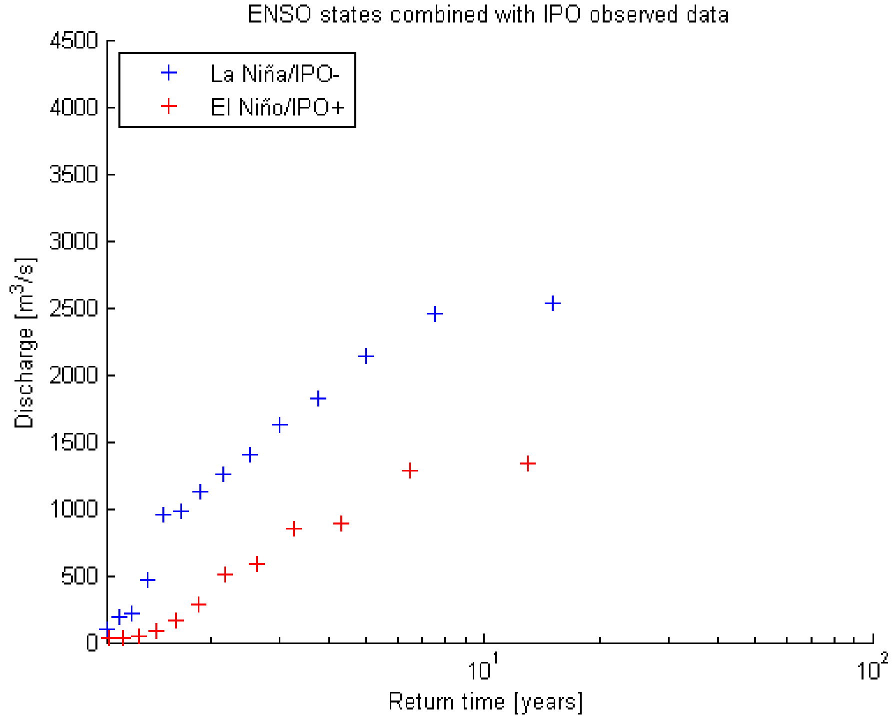

Figure F-6: Observed split data for IPO&ENSO positive and IPO&ENSO negative years

El Niño years in positive PDO years and La Niña years in negative PDO years

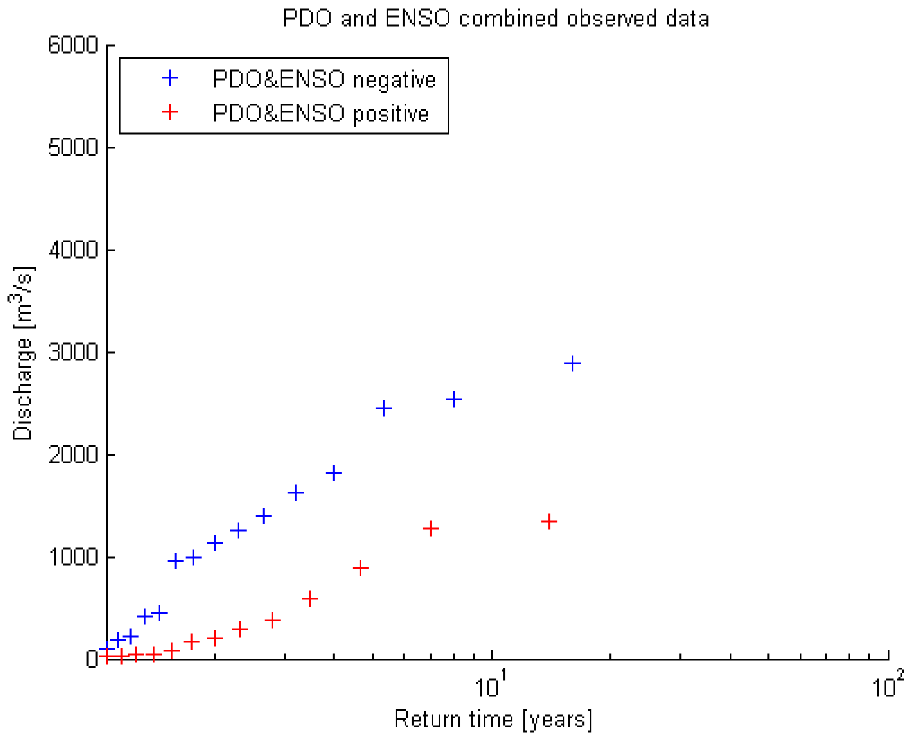

Figure F-7: Observed split data for PDO&ENSO positive and PDO&ENSO negative years

Appendix G. Tabulated values of unconditional and conditional flood frequency curves

G.1 Tabulated values of expected flood frequency curves

Expected flood events [m³/s]	Return Time [years]						
	2	5	10	20	50	100	200
Unconditional	546.2	1404.8	2007.6	2536.0	3111.7	3459.3	3739.9
IPO positive	497.4	1277.1	1871.8	2439.0	3123.8	3585.5	3997.0
IPO negative	802.5	1688.1	2117.3	2392.1	2596.4	2674.6	2713.5
PDO positive	343.3	853.7	1296.1	1777.9	2463.3	3010.6	3576.5
PDO negative	804.6	1840.8	2621.0	3380.0	4333.5	5008.9	5641.1
El Niño	244.1	812.5	1354.9	1955.4	2795.0	3439.5	4076.0
La Niña	814.0	1725.4	2460.1	3236.1	4320.0	5179.2	6067.7

G.2 Tabulated values of lower 95% confidence interval boundary lines

Lower 95% confidence limit [m³/s]	Return Time [years]						
	2	5	10	20	50	100	200
Unconditional	390.8	1142.6	1560.3	1712.8	1717.6	1658.7	1580.6
IPO positive	313.2	918.9	1312.6	1472.3	1459.9	1376.7	1271.6
IPO negative	476.4	1294.3	1374.6	1189.8	945.1	804.2	701.4
PDO positive	220.2	573.9	850.9	1065.4	1225.8	1271.6	171.4
PDO negative	507.0	1279.6	1792.9	2053.3	2095.0	2006.9	1872.8
El Niño	129.6	495.5	807.8	897.5	1028.6	977.1	894.6
La Niña	567.0	1229.3	1705.0	2083.7	2408.8	2542.1	2600.8

G.3 Tabulated values of upper 95% confidence interval boundary lines

Upper 95% confidence limit [m³/s]	Return Time [years]						
	2	5	10	20	50	100	200
Unconditional	763.5	1727.2	2583.0	3755.0	5637.1	7214.6	8848.7
IPO positive	789.9	1775.0	2669.3	4040.1	6684.2	9337.7	12564.0
IPO negative	1351.7	2201.7	3261.2	4809.3	7132.8	8884.6	10497.0
PDO positive	535.3	1269.9	1974.1	2966.8	4950.3	7127.8	10061.0
PDO negative	1276.8	258.1	3831.6	5564.2	8963.6	12502.0	16992.0
El Niño	459.8	1332.5	2272.5	3872.2	7594.9	12107.0	18572.0
La Niña	1168.5	2421.8	3549.7	5025.8	7747.8	10552.0	13156.0

Appendix H. IPO flood frequency curves without 1998 peak

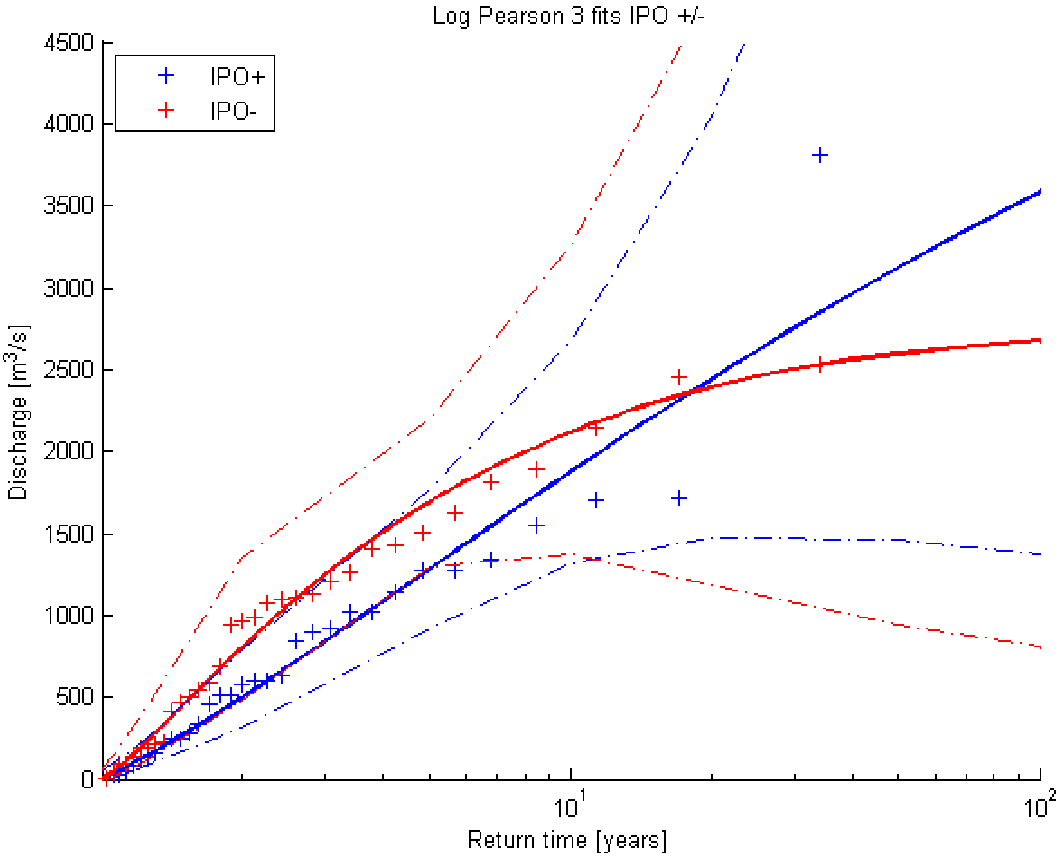

Figure H-1: IPO positive and negative flood frequency curves without 1998 IPO positive year discharge peak

Appendix I. HEC-RAS model calibration

As mentioned in the methodology (Chapter 4.4) the model is calibrated using rating curves. Figure I-1 shows the rating curves of the HEC-RAS steady flow analysis prior to and after model calibration. Also shown in Figure I-1 are the rating curves of DERM (Department of Environment and Resource Management, Queensland), BOM (Bureau of Meteorology, Australia) and the rating curve of the HEC-RAS model created by the Sunshine Coast Regional Council.

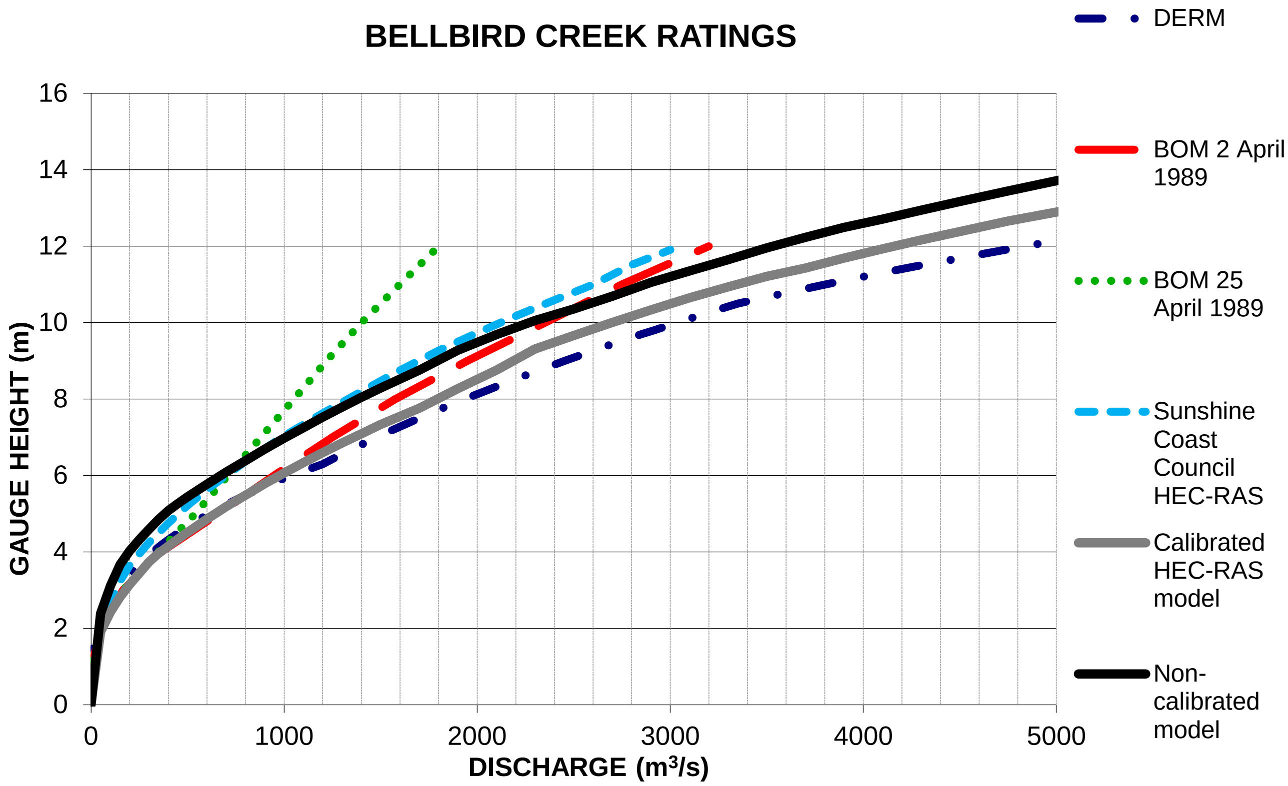

Figure I-1: Calibrated and non-calibrated model rating curves and DERM, BOM and SCC rating curves

The only change to the original model (bathymetry, roughness coefficients and steady flow conditions, see 4.4) was the external boundary condition, which was increased from a normal depth of 0.001 to 0.0015. This increase originates from the estimation of the water surface slope along the river reach in a run of the original model (0.0015 meter/meter river length) and as was stated in Chapter 4.4 the water surface slope is a good estimation for the normal depth boundary condition.

The reason to not calibrate towards one of the given rating curves (Figure I-1) is the great disagreement between the different organizations. Due to the differences between the rating curves a high uncertainty exists in what the true discharge-water height relation is for this river reach segment. Therefore the preferred model rating curve is somewhere in between. When conclusions are drawn from the inundation model it must be kept in mind that a great uncertainty exists in the rating curve.

Appendix J. Plots of flood inundation model outcomes

J.1 Cross-section plots of upstream boundary cross-section for 100 year flood events

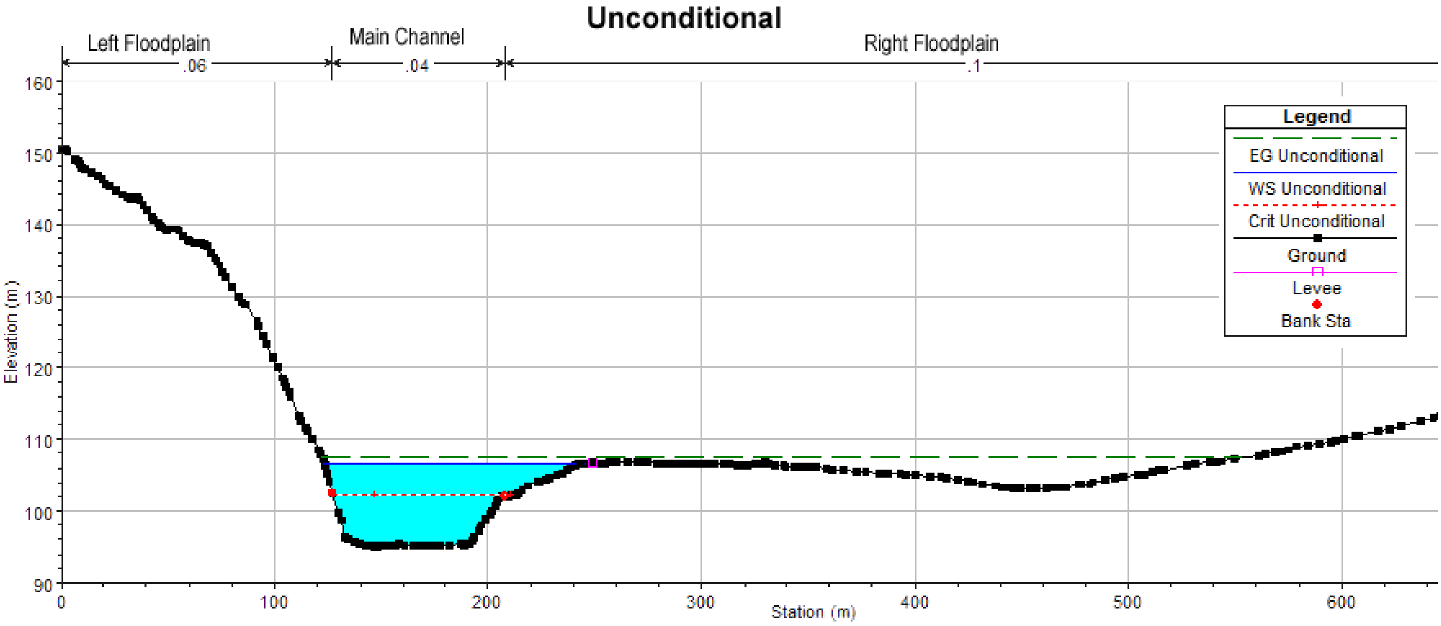

Figure J-I-1: Cross-section plot inundation due to unconditional 100 year flood event

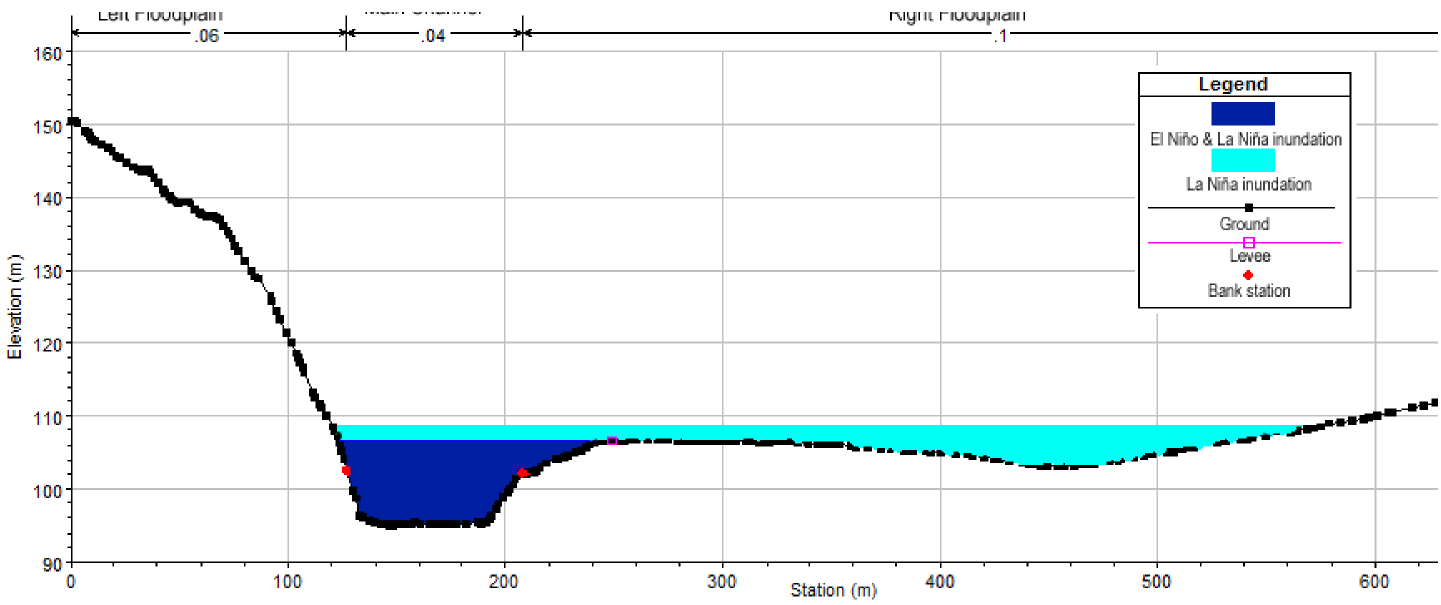

Figure J-2: Cross-section plot inundation due to La Niña and El Niño 100 year flood events

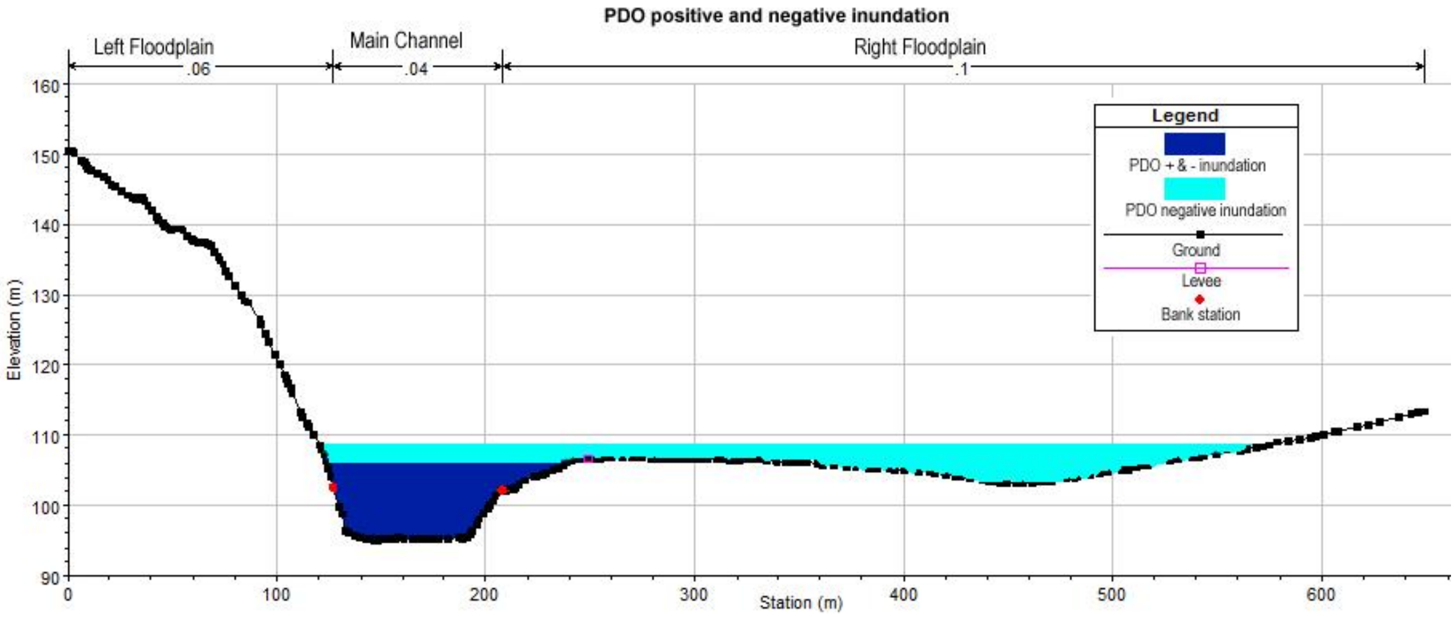

Figure J-3: Cross-section plot inundation due to PDO positive and negative 100 year flood events

J.2 95% uncertainty levels due to climate variability: 3-D plots

The discharges corresponding to the 95% uncertainty limits at a data length of 200 years are $2.7 * 10^3$ and $5.3 * 10^3 m^3/s$, see Chapter 5.2.

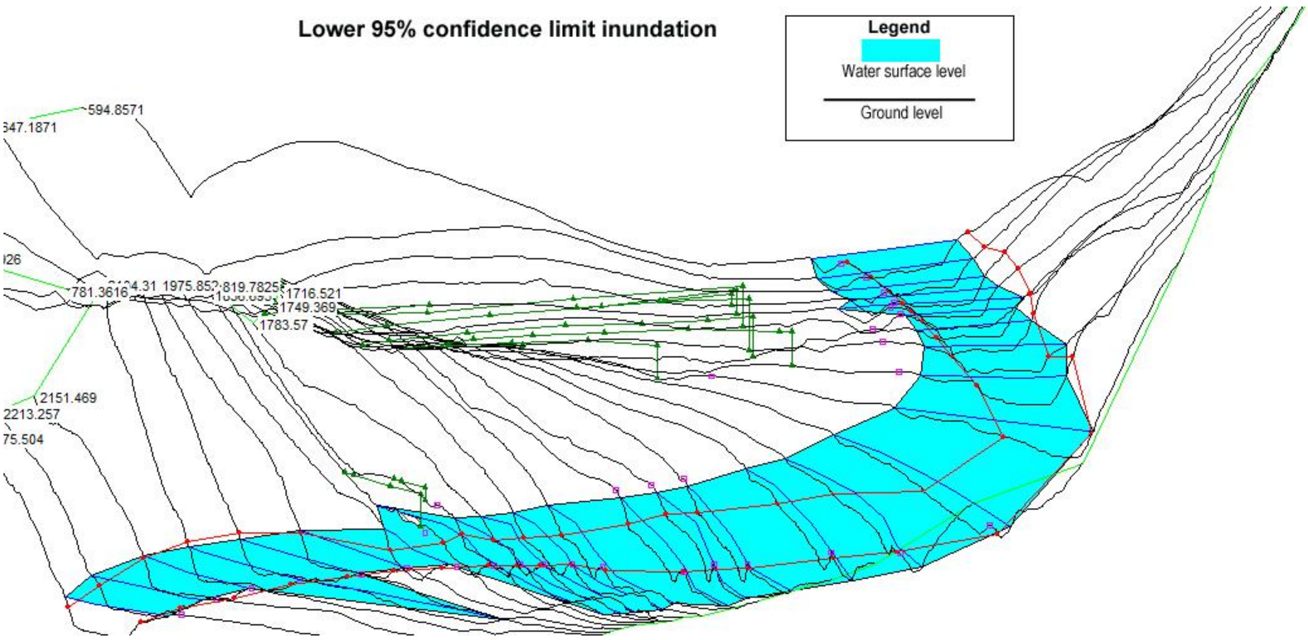

Figure J-4: Lower 95% confidence limit 100 year flood 3-D plot of inundation

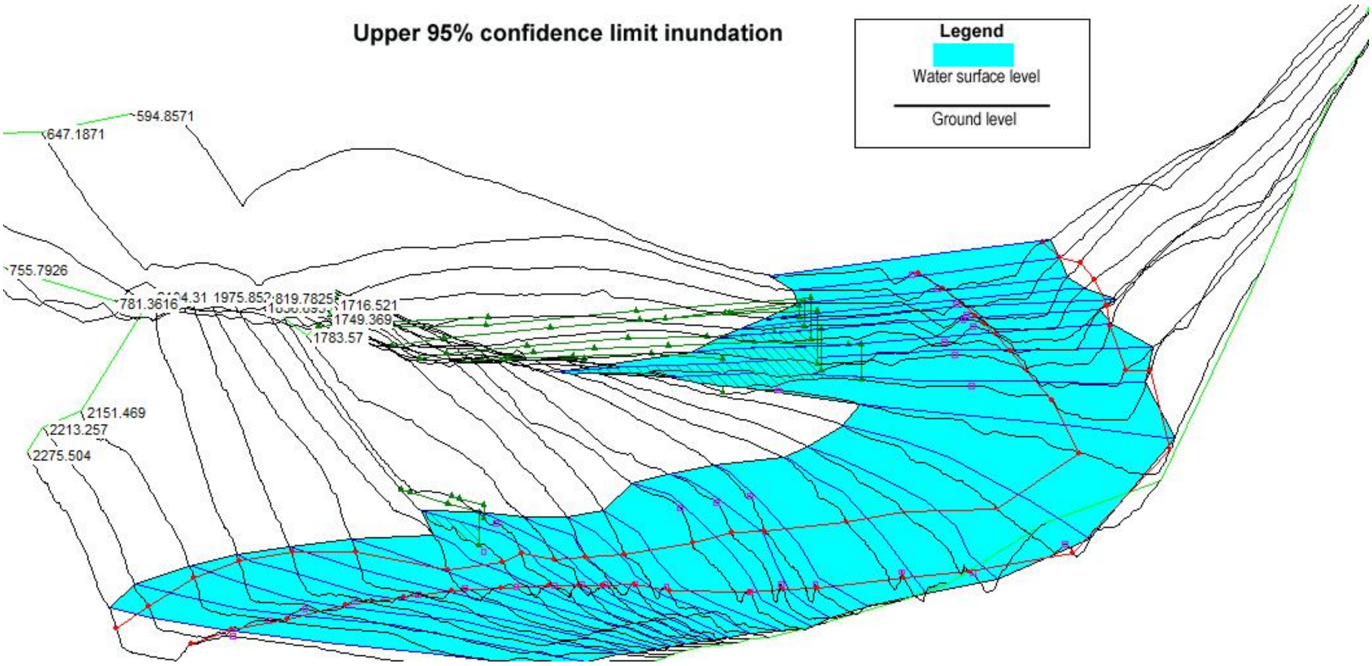

Figure J-5: Upper 95% confidence limit 100 year flood 3-D plot of inundation

Appendix K. Data analysis for Clarence River Catchment

The Clarence River catchment area shows the strongest IPO signal of the selected catchments (Chapter 5.4). This appendix shows the (visual) results of the flood frequency analysis for this gauge in New South Wales. The graphs and tables in this appendix are listed below:

Table K-1: P- values of climate state discharges

- Table K-2: 100 year flood magnitudes Clarence River
- Figure K-1: Distribution model fits
- Figure K-2: Unconditional Log-Pearson type 3 fit
- Figure K-3: IPO positive and negative stratification
- Figure K-4: Plots IPO positive phases
- Figure K-5: PDO plots
- Figure K-6: ENSO plots
- Figure K-7: IPO&ENSO positive and IPO&ENSO negative
- Figure K-8: PDO&ENSO positive and IPO&ENSO negative
- Figure K-9: Uncertainty in 100 year flood estimation due to IPO variability
- Figure K-10: Uncertainty in 100 year flood estimation due to ENSO variability

K.1 Discussion of results Clarence River catchment

The Clarence River catchment clearly has very strong climate variability signals. Firstly the IPO strength is 2.55 (100 year floods). The individual phases have rather similar deviations from the mean unconditional situation, the negative and positive phases respectively wielding a 100 year flood 1.49 and 0.59 times the unconditional 100 year flood. A further proof of the good distinction between the phases is the calculated p-values. A comparison between the positive and the negative phase results in a p-value of 0,000(5), indicating a very significant chance the means of the series are different. Furthermore in a comparison of the two positive phases (1920-1944 and 1978-1998) a p-value of 0.792 is calculated. Along with the graphical plot in Figure K-4 this indicates a very similar flood frequency curve. Altogether it can be said all parameters indicate a very clear IPO signal and the characteristics of the IPO are visible.

Secondly the PDO also has a strong signal in the Clarence River catchment. By again stratifying the data in three phases with a threshold for the positive and negative phase of 0.5 and -0.5 times the standard deviation, a strong signal is visible in the graphical plot as well as the p-value. The PDO strength for 100 year floods is 2.08. The PDO's positive and negative phases have rather similar deviations and the neutral phase wields nearly the same 100 year flood event as the unconditional flood event. Just like for the IPO this means the PDO has a clear distinction and expected characteristics. The p-value for the positive and the negative phase is 0.003, again indicating a significant difference in means.

Of further interest is the similarity between the IPO and the PDO, which has been described in Chapter 2.2 and investigated for the Upper Mary River catchment in the results section. Contradictory to the Upper Mary River catchment, the Clarence River catchment does have a strong agreement between the effects of the IPO and the PDO. Firstly the values of the 100 year floods are fairly similar: 8674.2 and 8329.4 m^3/s for the negative states and 3405.3 and 3999.7 m^3/s for the positive states. Furthermore the form of the model fits and the uncertainty bounds are comparable.

Besides the (multi-)decadal variability the ENSO also has a fairly strong signal in this catchment, with an ENSO strength of 1.74 for 100 year floods. Whereas in the Upper Mary River catchment El Niño events do not alter the flood frequency significantly, the effects of El Niño are visible in the Clarence River catchment, lowering the 100 year flood event to 75 % of the unconditional event. A further notable result is the Nino3.4 index wielding both the highest ENSO strength (1.74 versus 1.42) and the lowest p-values (0.052 versus 0.104). This again proves the MEI is not always the best identifier for ENSO events (see results of Question 2 in Chapter 5).

Combining the climate variability modes does alter the flood frequency curves significantly in contrast to the Upper Mary River catchment, both for the combination of IPO as PDO with the ENSO. The P-values are very low and the strengths of those combined events wield the lowest and highest 100 year floods. Again the IPO and the PDO have rather similar effects.

Finally the uncertainty analysis using a Monte Carlo simulation shows comparable results for the Clarence River as for the Upper Mary River. Besides analysing the uncertainty due to ENSO the IPO variability can be considered, since the IPO has a strong signal in this catchment. For the Clarence River the uncertainties due to both the IPO and the ENSO individually are particularly high for short data lengths and remain fairly large for longer data lengths.

Table K-1: P- values of climate state discharges

	P-value
IPO positives and negative	0.000
IPO positives 1920-1944 & 1978-1998	0.792
PDO positive and negative	0.003
El Niño and La Niña	0.052
ENSO&IPO positive and ENSO&IPO negative	0.001
ENSO&PDO positive and ENSO&PDO negative	0.002

Table K-2: 100 year flood magnitudes Clarence River

	100 year flood [m^3/s]	Percentage of unconditional flood frequency [%]
Unconditional	5805.5	100
IPO positive	3405.3	59
IPO negative	8674.2	149
PDO positive	3999.7	69
PDO neutral	5863.6	101
PDO negative	8329.4	143
ENSO positive (El Niño)	4334.8	75
ENSO neutral	6386.4	110
ENSO negative (La Niña)	7526.4	130
IPO positive/ENSO positive	2078.9	36
IPO negative/ENSO negative	9064.0	156
PDO positive/ENSO positive	2119.3	37
PDO negative/ENSO negative	9467.0	163

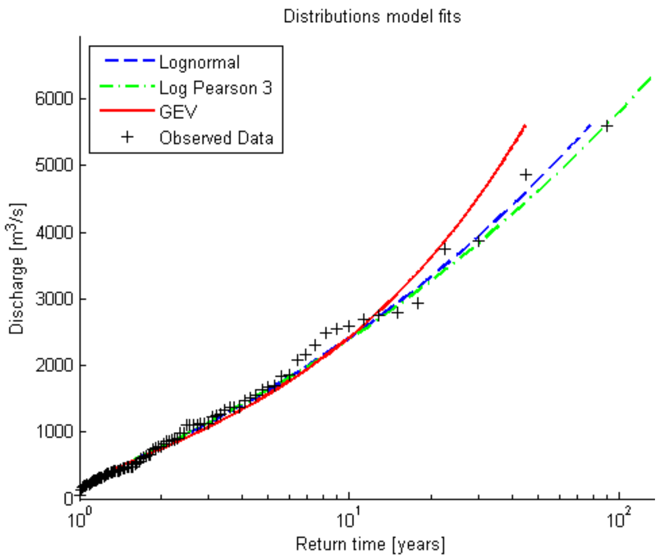

Figure K-1: Distribution model fits

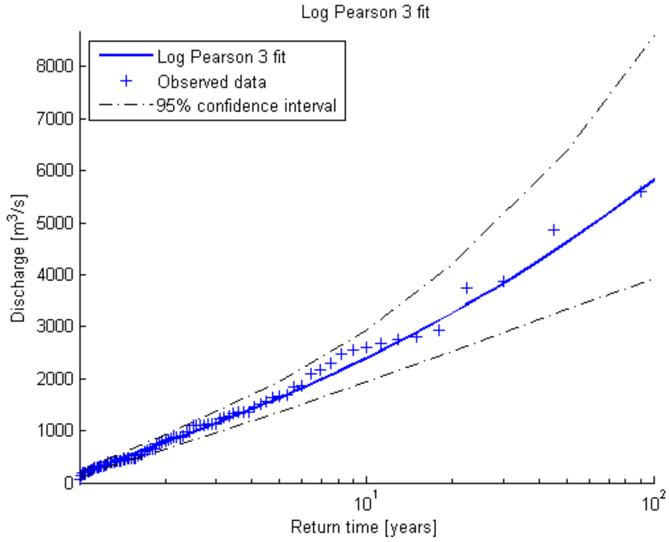

Figure K-2: Unconditional Log-Pearson type 3 fit

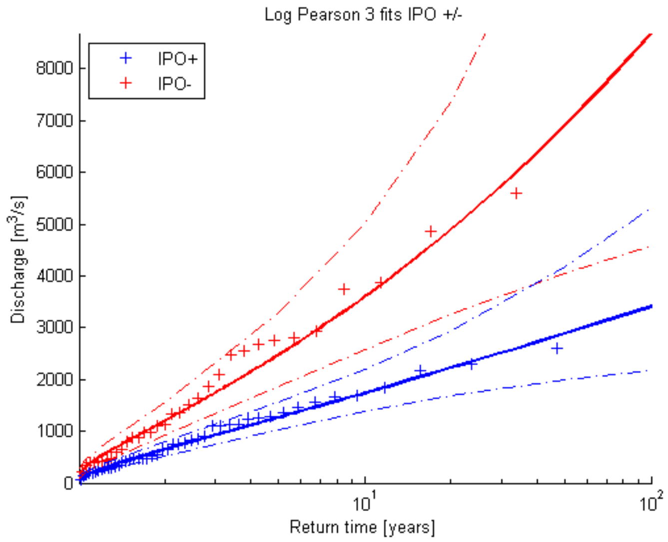

Figure K-3: IPO positive and negative stratification

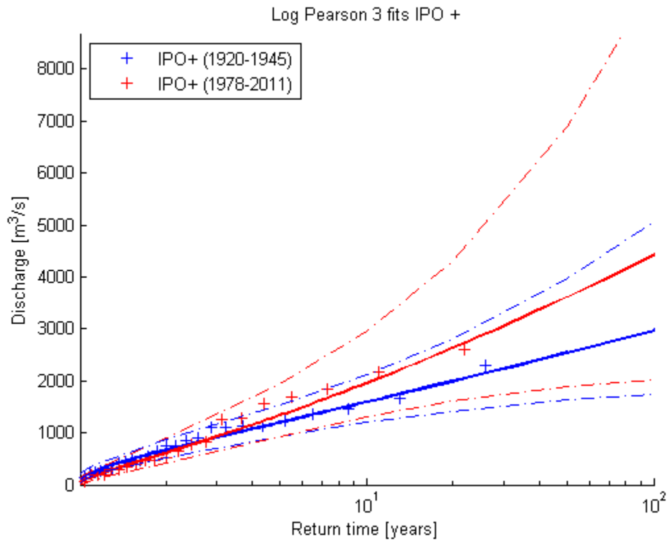

Figure K-4: Plots IPO positive phases

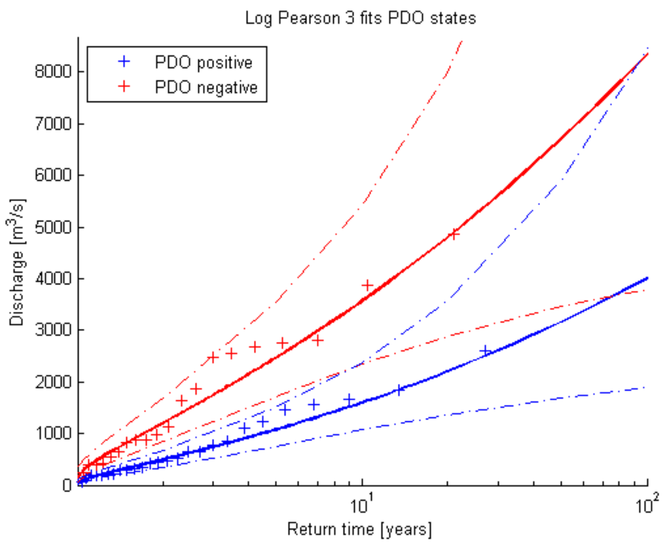

Figure K-5: PDO plots

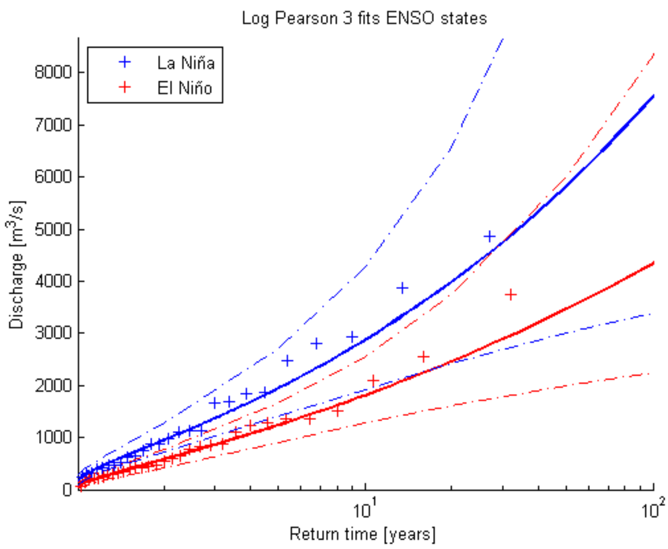

Figure K-6: ENSO plots

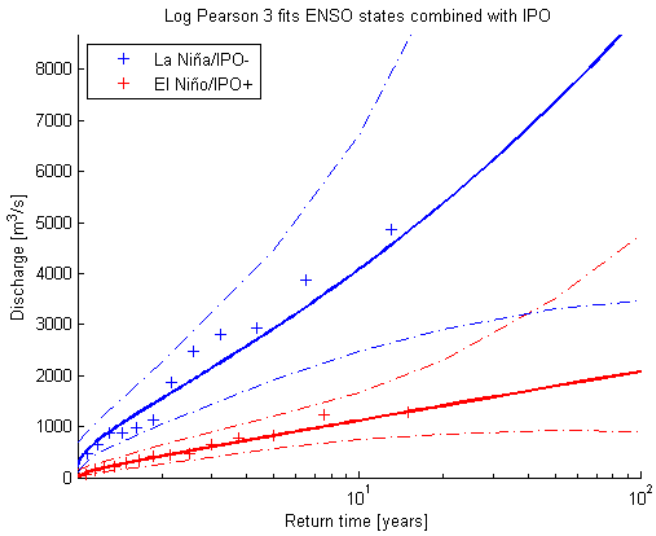

Figure K-7: IPO&ENSO positive and IPO&ENSO negative

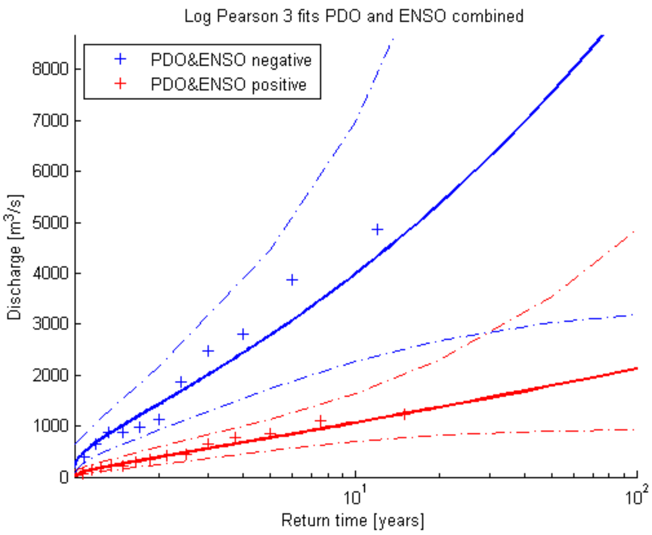

Figure K-8: PDO&ENSO positive and IPO&ENSO negative

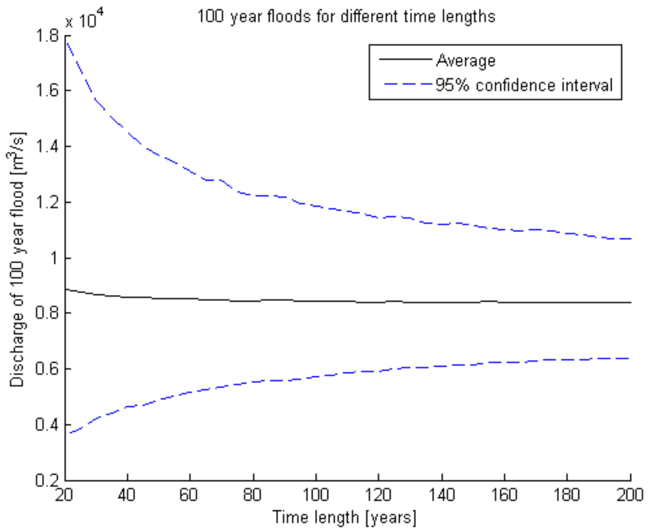

Figure K-9: Uncertainty in 100 year flood estimation due to IPO variability

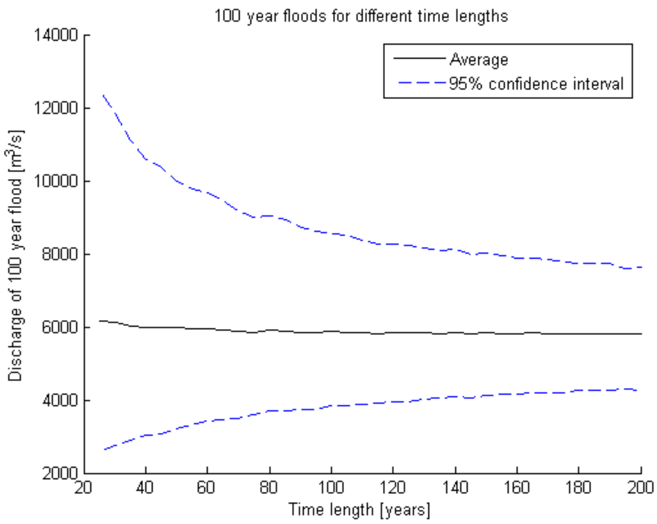

Figure K-10: Uncertainty in 100 year flood estimation due to ENSO variability